Physics – Uspekhi **47** (6) 533 – 554 (2004)

REVIEWS OF TOPICAL PROBLEMS PACS numbers: **71.30.+h**, 71.45.Lr, 73.63.Nm

Finite-size effects in quasi-one-dimensional conductors with a charge-density wave

S V Zaĭtsev-Zotov

DOI: 10.1070/PU2004v047n06ABEH001675

Contents

Abstract. Recent studies of finite-size effects in charge-density wave conductors are reviewed. Various manifestations of finite-size effects, including the transverse-size dependence of the nonlinear-conduction threshold field, the Peierls transition temperature, high-frequency conduction, and the relaxation rates of metastable states, are discussed. Resistivity jumps in thin samples, the smeared threshold field for nonlinear conduction, and threshold conduction above the Peierls transition temperature are considered, as are mesoscopic oscillations of the threshold field, one-dimensional conduction in thin crystals, absolute negative conductivity of quan-one-dimensional conductors, the length dependence of the phase-slip voltage, and the Aharonov – Bohm oscillations in sliding CDWs. Problems yet to be solved are discussed.

1. Introduction

Recent years have seen an upsurge in interest in the physics of one-dimensional systems and in charge-density waves (CDWs) in low-dimensional systems. This is due to the appearance of new areas of research brought to life by the discovery of charge-ordered and stripe phases and to advances in modern technology, which have made it possible to fabricate objects with a one-dimensional, or close to one-dimensional, electron spectrum. It must be noted, however, that CDWs in quasi-one-dimensional conductors have been studied for more than two decades, and the physical properties of these materials have been well documented. The reviews in Ref. [1], published mainly in the late 1980s or early 1990s, give a fairly detailed picture of the general properties of quasi-one-dimensional conductors with CDWs. Since then, the knowledge about the physics of CDWs has become much deeper and the physics of quasi-one-dimensional conductors has gotten richer with new interesting observations. In particular, more than a dozen different finite-size effects have been discovered in the kinetics of CDWs. The studies of finite-size effects have provided knowledge about correlation lengths, and new mechanisms of relaxation of metastable states have been proposed. The study of finite-size effects has stimulated the building of a semiconductor model of quasi-one-dimensional conductors and demonstrated the need to use two potentials in describing the kinetic properties: the electrochemical potential, which determines the kinetics of the quasiparticles, and the electrostatic potential, which determines the CDW kinetics. Moreover, thanks to the development of new techniques for fabricating structures based on quasi-one-dimensional conductors with CDWs, it has become possible in recent years to study CDW kinetics in the nanometer scale. All this points to the need to summarize the results of the previous stage in studying quasi-one-dimensional conductors with CDWs and, in particular, finite-size effects in these materials. The goal of the present review is to acquaint the reader with the main finite-size effects known to exist in the

S V Zaĭtsev-Zotov Institute of Radio Engineering and Electronics, Russian Academy of Sciences
ul. Mokhovaya 11, korp. 7, 125009 Moscow, Russian Federation
Tel. (7-095) 203 47 17, (7-095) 203 49 87
Fax (7-095) 203 84 14
E-mail: serzz@cplire.ru

Received 14 May 2003
Uspekhi Fizicheskikh Nauk **174** (4) 585 – 608 (2004)
Translated by E Yankovsky; edited by M V Chekhova

physics of quasi-one-dimensional conductors. In view of the narrow selection of themes, the review does not cover all the aspects of the physics of quasi-one-dimensional conductors. The current state of studies in this area of research has been covered rather fully in the proceedings of various conferences devoted to electronic crystals [2]. A detailed discussion of finite-size effects that emerge in $NbSe_3$ samples as their cross section gets smaller is given in the report by R E Thorne's group (see Ref. [3]). Among the reviews devoted to other aspects of the physics of quasi-one-dimensional conductors with CDWs we would like to mention the one by Brill [4] on the elastic properties of quasi-one-dimensional conductors and the review by Latyshev and Sinchenko [5] who considered the experiments involving mesoscopic structures built from quasi-one-dimensional conductors with CDWs.

The plan of the review is as follows. Section 2 is a brief introduction into the physics of quasi-one-dimensional conductors with CDWs. Attention is focused on the most general physical properties of such materials and the main ideas that are used to describe the properties and are important for understanding the finite-size effects discussed in the review. Section 3 is a discussion of finite-size effects and their physical interpretation. At the end of that section, in Sections 3.11 – 3.15, we examine several unresolved problems related to finite-size effects and the physics of quasi-one-dimensional conductors.

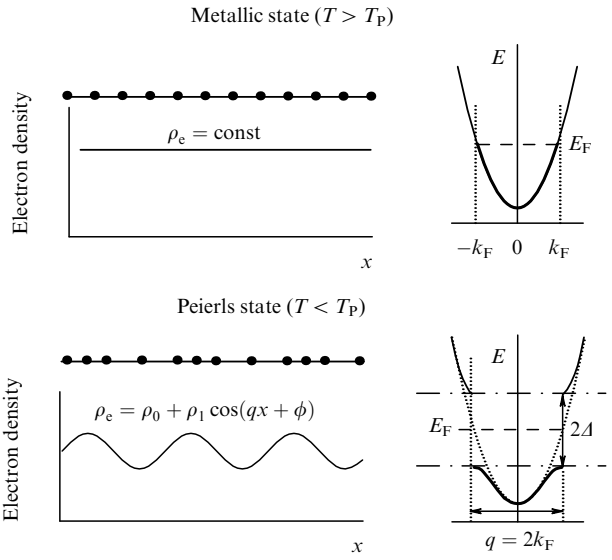

Figure 1. The origin of a Peierls transition in a one-dimensional metal. The upper part of the figure shows the positions of atoms in the metallic chains, the distribution of the electron density along the metallic chains, and the energy spectrum of the initial metal. The lower part illustrates the same situation but in a Peierls metal. The heavy curves in the energy spectra denote the states occupied by electrons.

2. The main properties of quasi-one-dimensional conductors with a charge-density wave

2.1 The origin of CDWs

A charge-density wave can appear in various materials. For example, it is observed in metals of the chrome type, which have a three-dimensional energy spectrum, in layer structures like dichalcogenides of transition metals MX_2 (M = Nb, Ta, X = Se, S), which have quasi-two-dimensional energy spectra, in a large class of inorganic quasi-one-dimensional conductors like tri- and tetrachalcogenides of transition metals MX_3 and MX_4 (M = Nb, Ta, X = Se, S), so-called blue bronzes $M_{0.3}MoO_3$ (M = Rb, K), $(TaSe_4)_2I$, and many others. Most interesting are inorganic quasi-one-dimensional conductors in which the charge-density wave can slide, thus contributing to the electric current, which leads to many unusual effects. The present review is devoted to the properties of just such compounds.

The simplest way to illustrate the appearance of a CDW is to examine a one-dimensional metal, whose structure is depicted in Fig. 1. A periodic distortion of the crystal lattice with a wave vector q equal to twice that of the wave vector of the electrons on the Fermi surface, k_F, leads to the formation of an energy gap 2Δ at the Fermi level, which, naturally, lowers the energy of the electron system of the one-dimensional metal. Here, the energy cost of the deformation of the crystal lattice proves to be somewhat smaller than the energy gain of the electron system [1], which makes such a state preferable energywise.

A charge-density wave appears when the temperature decreases as a result of the phase transition known as the Peierls transition. The emerging state is characterized by periodic modulation of both the positions of the lattice atoms and the electron density $\rho_e = \rho_0 + \rho_1 \cos(qx + \phi)$, where ρ_0 and ρ_1 are the mean value and the modulation amplitude of the electron density, respectively, $q = 2k_F$ is the CDW wave vector, and ϕ is the CDW phase, and a Peierls gap of 2Δ appears in the electron spectrum. The characteristic scale of the atomic displacements in the lattice is 0.05 Å [7]. The charge-density wave is characterized by a complex order parameter $\Psi = \Delta \exp(i\phi)$. In the absence of defects and impurities and in the case where the CDW wave vector and the crystal lattice are incommensurable, the phase ϕ and Δ and, hence, the CDW energy are independent of x, i.e., there is translation invariance. Because of such invariance, a CDW can move along the x axis, which is described by in the time dependence of the phase, $\phi(t) = \phi(0) + \omega t$. Such motion is accompanied by the transport of the electric current (the Fröhlich conduction).

The interaction between a CDW and impurities destroys long-range order, disrupts translation invariance, and leads to a finite phase correlation length [8 – 11], which is often called the Fukuyama – Lee – Rice length and, since recently, also the Larkin length. As a result, a CDW slides only when the electric field E is higher than a certain value E_T, which is usually called the threshold field for the onset of nonlinear conduction.

The periodic charge-density modulation inherent in CDWs leads to a narrow-band noise appearing in the course of CDW sliding. The noise frequency is proportional to the speed of the CDW motion. Application of a radio-frequency (RF) field results in steps appearing in the current-voltage characteristics at positions where the narrow-band noise frequency is multiple to the RF frequency (Shapiro steps). In electric fields weaker than the threshold field, the CDW is pinned, and its polarizability is characterized by an enormous dielectric constant, $10^7 – 10^8$. The typical values of the threshold field in the purest samples are 10 – 100 mV cm^{-1}.

$NbSe_3$ and orthorombic TaS_3 are among the quasi-one-dimensional conductors that have been studied most thoroughly. Below we list the main physical properties of these compounds.

[1] The first to notice this was Peierls [6].

Orthorombic TaS_3 (from now on simply TaS_3) is a typical quasi-one-dimensional conductor in which, as a result of a Peierls transition, the electron spectrum undergoes complete dielectrization [1]. In the metallic state, TaS_3 is a highly anisotropic metal with a conductivity along the chains approximately 200 times higher than that in the transverse directions. The Peierls transition temperature is $T_P = 220$ K, and the characteristic nonlinear-conduction threshold field for pure samples $E_T < 1$ V cm^{-1}. At temperatures $T > T_P$ the conduction is metallic, while at $T < T_P$ it is of the activation type, with the activation energy $\Delta \approx 800$ K. Usually, the transition temperature is assumed to be the value at which the derivative $d \ln R/d(1/T)$ reaches its maximum (R is the resistance). The crystal lattice is orthorombic, and the CDW wave vector has components close to ($1/2a^*$, $1/8b^*$, $1/4c^*$), where a^*, b^*, and c^* are the unit cell parameters, which, however, differ by several percents from those corresponding to exact commensurability. Here, the component of the CDW wave vector along the axis of the highest conductivity, c^*, depends on the temperature, decreasing by 1–2% as the temperature drops from 220 to 100 K [12]. The temperature dependence of the wave vector leads to a temperature hysteresis of the conductivity [13], the scale of which can exceed 40%.

The $NbSe_3$ compound has two Peierls transitions at $T_{P1} = 145$ K and $T_{P2} = 59$ K and occupies a special place among quasi-one-dimensional conductors with a CDW because of incomplete dielectrization of the electron spectrum at $T < T_{P2}$, which ensures the preservation of metallic conduction at zero temperature [1]. The crystal lattice is monoclinic, with the direction b^* coinciding with that of the highest conductivity. In the metallic state the conductivity along the b^* axis is roughly 20 times higher than that along the a^* axis and, apparently, is almost 1000 times higher than along the c^* axis. The wave vector of the low-temperature CDW has the components (0, 0.243, 0), while the wave vector components of the high-temperature CDW are (0.5, 0.259, 0.5). The electron concentration in the metallic state is $n_e = 3.8 \times 10^{21}$ cm. As a result of the high-temperature transition, the concentration of free carriers decreases by a factor of almost two, while after the second Peierls transition a small fraction of metallic electrons with a concentration $n_e \approx 6 \times 10^{18}$ cm^{-3} [14] remains in the metallic state at zero temperature. Typical values of the threshold field for pure samples are ~ 0.1 V cm^{-1} for a high-temperature CDW and are smaller than 10 mV cm^{-1} for a low-temperature CDW.

2.2 CDW pinning

2.2.1 CDW phase correlation length. When a CDW gets captured by impurities, we speak of CDW pinning. Pinning destroys long-range order in the CDW, which leads to a situation in which the phase correlation length is finite [8–11].

Two types of pinning are distinguished. In the case of strong pinning, the CDW interacts with each impurity independently. The threshold field at which CDW sliding begins proves to be proportional to the concentration of strong pinning centers. In the case of weak (collective) pinning, one should take into account the elastic deformation energy of the CDW. The CDW deforms to minimize the energy of interaction with impurities. CDW deformation can be described as a position-dependent CDW phase, $\phi(x)$, or, alternatively, as a position-dependent wave vector, $q(x)$.

The first to calculate the correlation length for quasi-one-dimensional conductors with CDWs were Efetov and Larkin [9]. For the correlator of the order parameter they obtained the following expression:

$$\langle \Psi(0)\Psi^*(\mathbf{r})\rangle = \Delta^2 \exp\left(-\left\langle \phi(0)\left[\phi(0)-\phi(\mathbf{r})\right]\right\rangle\right) = \Delta^2 \exp\left(-\sqrt{\frac{x^2}{L_\parallel^2}+\frac{\rho^2}{L_\perp^2}}\right),$$

where x and ρ are the components of the vector $\mathbf{r}$ along and perpendicular to the chains, respectively, $L_\parallel$ and $L_\perp$ are the corresponding phase correlation lengths ($L_\parallel = \alpha L_\perp$, with α being the anisotropy coefficient, $\alpha > 1$). In its turn, the longitudinal phase correlation length was found to be

$$L_\parallel = \frac{4\pi K_\parallel^2}{w_i^2 n_i},$$

where $K_\parallel$ is the CDW elasticity modulus along the chains, w_i is the CDW–impurity interaction potential, and n_i is the impurity concentration.

An alternative method commonly used to estimate the correlation length was developed by Fukuyama, Lee, and Rice [10, 11]. This method is based on the following considerations. The deformation of the CDW leads to a gain in the energy of interaction with the impurities, W_p, at the expense of a certain amount of elastic-deformation energy W_{el}. If L is the characteristic spatial scale of the correlation length the average energy density of CDW deformation can be estimated as

$$W_{el} \sim \frac{1}{2} K\left(\frac{\pi}{L}\right)^2,$$

and the pinning energy density, as

$$W_p \sim w_i \frac{\sqrt{n_i L^D}}{L^D},$$

where K is the CDW elastic modulus in the isotropic representation, and D is the dimensionality of the space. Minimization of the difference of these energies in L yields the following estimate:

$$L \sim \left(\frac{K^2}{w_i^2 n_i}\right)^{1/(4-D)}. \quad (1)$$

2.2.2 The threshold field of the onset of the CDW sliding. In an electric field a CDW can slide along the x axis, thus transporting the electric current (the Fröhlich conduction). This sliding is described by the time dependence of the phase, $\phi(t) = \phi(0) + \omega t$. Due to the interaction with the imperfections of the crystal lattice and impurities, CDW sliding emerges only when $E > E_T$.

In the case of weak pinning, the threshold field can be estimated in the Fukuyama–Lee–Rice model by assuming that the displacement of the CDW by approximately one period changes the pinning energy by a value on the order of W_p [11]. Such an estimate yields

$$E_T \sim \frac{q}{e\rho_0}\left(\frac{w_i^4 n_i^2}{K^D}\right)^{1/(4-D)}. \quad (2)$$

Sometimes, in making estimates it is more convenient to use the simpler (but equivalent) relationship

$$E_T \sim \frac{s_0}{e}\frac{K}{L^2}, \quad (3)$$

where s_0 is the area per unit chain.

It is interesting to consider the mechanism of energy dissipation during CDW sliding. In the absence of impurities, the existence of quasiparticles leads to a bare dissipation, which, however, is small [15]. The situation changes crucially when there are impurities [16]. The interaction with impurities distorts the CDW. When the CDW is sliding, its deformation is time-dependent, which generates flows of quasiparticles that screen the internal fields. The quasiparticle motion leads to the energy dissipation. As a result, the "CDW conductivity", i.e., the field-dependent coefficient γ in the equation for the collective current $I_c = \gamma(E - E_T)$, proves to be proportional to the conductivity σ caused by the quasiparticles (electrons and holes). The most important consequence of all this is the occurrence of a strong temperature dependence of the coefficient γ similar to the temperature dependence of linear conductivity $\sigma(T)$ [17].

As noted earlier, both the CDW and the quasiparticles (electrons and holes thermally excited through the Peierls gap) participate in the transport of electric current. The current transported by quasiparticles is determined, as it is in ordinary semiconductors, by the difference in the levels of electrochemical potential. At the same time, CDW motion depends on the strength of the electric field, i.e., on the gradient of the electrostatic potential. Since CDW deformation leads to a shift in the chemical potential, quasi-one-dimensional conductors with a nonuniform impurity distribution in space manifest exotic features such as the existence of absolute negative resistance [18].

CDW deformation, i.e., deviation of the CDW wave vector from its equilibrium value, causes an increase in the energy of the quasi-one-dimensional conductor. The equilibrium value of the CDW wave vector can be found from the minimum condition imposed on the free energy of a Peierls conductor. In the simplest case of a linear energy spectrum, $E = kv_F$, the equilibrium value $q = 2k_F$ is temperature-independent. For real quasi-one-dimensional conductors, the curvature of the dependence $E(k)$ leads to a deviation in the equilibrium value of q from $2k_F$ and to the occurrence of a temperature dependence $q(T)$ close to the activation type [19]. For instance, typical temperature variations of q in $NbSe_3$, TaS_3, and $K_{0.3}MoO_3$ prove to be about 1%.

2.2.3 The rigid-CDW model and the dielectric constant of quasi-one-dimensional conductors. Another manifestation of CDW pinning is the huge dielectric constant of quasi-one-dimensional conductors (on the order of $10^7 - 10^8$) and the strong frequency dependence of AC conductivity. The low-frequency dielectric constant and its frequency dependence can be estimated by using a simple model, in which a rigid CDW moves in a periodic pinning potential $W_p \sin(\phi(t))$ when an electric field is applied to the system. Within this model one can find the shape of the current – voltage characteristics and the threshold field $E_T = qW_p e\rho_0$ [20, 21]. For the real and imaginary parts of the collective conductivity we have the following equations:

$$\mathrm{Re}\,\sigma = \frac{\rho_0 e^2}{\gamma m^*} \frac{\omega^2}{\omega^2 + \omega_0^2}, \tag{4}$$

$$\mathrm{Im}\,\sigma = \frac{\rho_0 e^2}{\gamma m^*} \frac{\omega\omega_0}{\omega^2 + \omega_0^2}, \tag{5}$$

where

$$\omega_0 = \frac{e\rho_0 q E_T}{\gamma m^*}. \tag{6}$$

Here, m^* is the effective CDW mass, and γ describes the dissipation of energy during CDW motion [21]. These equations predict a maximum in conductivity at a frequency ω_0 proportional to the threshold field, which is in good agreement with the experimental data [22]. For the low-frequency dielectric constant ϵ, equation (5) yields the following simple relation: $\epsilon = e/qE_T$. This implies that the low-frequency dielectric constant is equal, by order of magnitude, to the ratio of the interatomic electric fields to the threshold field, which explains its large value observed in experiments.

2.2.4 Pinning with allowance for local CDW deformation. The classification of types of pinning proves to be richer if we allow for both collective pinning and local deformation of the CDW [23]. Taking these local distortions into account, we find that the pinning force exerted by the jth impurity can be written in the form $F_j = w_i q \cos(qr_j + \phi + \delta\phi_j)$, where ϕ is the macroscopic phase, and $\delta\phi_j$ is the local distortion, $\delta\phi_j = \phi_j - \phi$, with ϕ_j being the CDW phase on the jth impurity. The local distortion, in its turn, can be found from the equation

$$\delta\phi_j = \frac{\alpha F_j}{w_i q}, \tag{7}$$

where α is the dimensionless measure of local deformability of the CDW. As a function of the macroscopic CDW phase, the pinning potential at $\alpha < 1$ is already not sinusoidal, but the mean value of the force is still equal to zero, which ensures weak CDW pinning.

The value $\alpha = 1$ is the point after which strong pinning sets in: for higher values there is hysteresis in the dependence of the pinning potential on the macroscopic phase and the mean contribution of the pinning centers in the course of CDW sliding becomes nonzero (Fig. 2). The threshold field now incorporates the contribution of weak pinning, approximately proportional to $N^{1/2}$, with $N = n_i L^D$, and the contribution of strong pinning, approximately proportional to N.

Such a model is widely used to describe various phenomena related to CDW pinning and agrees well with the results of experiments [24 – 27].

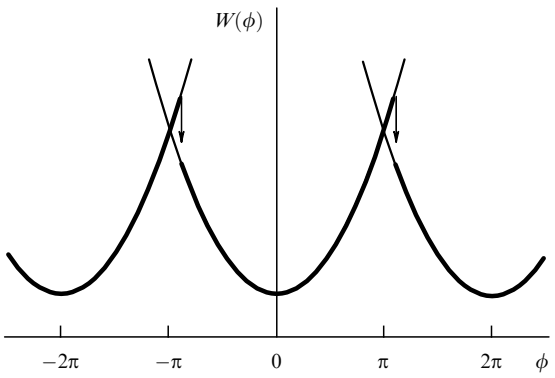

Figure 2. Pinning potential with an account for the local deformation of a CDW as a function of the macroscopic CDW phase [23]. The heavy curve depicts the path of motion along the potential when the CDW slides at a finite temperature.

The characteristic phase correlation lengths in typical quasi-one-dimensional conductors with CDWs, $NbSe_3$ and TaS_3, prove to be on the order of 1 μm in the direction perpendicular to the chains [28] and on the order of 10 μm in the direction parallel to the chains [29]. Here, the accuracy with which correlation lengths are measured along the chains by X-ray analysis is limited by lengths on the order of 1 μm. The conclusion that there can be much longer phase correlation lengths is based on the studies of sudden changes of the CDW phase performed by the thermal probe method [29].

2.3 CDW creep

Since at finite temperatures the barriers related to pinning can be surmounted due to thermal fluctuations, CDW motion is possible even if $E < E_T$. Here, the speed of such motion is determined not by the rate of energy dissipation, as when CDWs slide, but by the rate of pinning energy barriers surmounting. Such a mode of motion is called CDW creep.

CDW creep can be observed at high temperatures in small samples of quasi-one-dimensional conductors, where CDW fluctuations become so large that one can observe the contribution from spontaneous CDW motion. For more details on this type of creep see Section 3.6, which is devoted to finite-size effects near Peierls transitions [3, 26].

Another way to observe CDW creep is to study the nonlinear conduction at low temperatures, when all the electrons and holes freeze out and it becomes possible to measure very weak CDW currents in sufficiently high electric fields [30].

Following Nattermann [31], consider the displacement of a CDW along the chains over a small distance δx along the direction of the electric field. This displacement causes a deformation of the CDW within a volume L^D, with $L \sim \delta x^{\xi}$ $(0 < \xi < 1)$ [31]. The energy increase due to the CDW's displacement along the field proves to be equal to $\rho_e E \delta x L^D$, where ρ_e is the CDW charge density, while the energy cost of the CDW's deformation can be estimated as $KL^D(\delta x/L)^2$. This implies that there is a maximum barrier height for CDW creep, $W \propto 1/E^a$, with $a = (D - 2 + 2\xi)/(2 - \xi)$ [31], which determines the activation energy for the CDW current I_c at $E < E_T$ in the case of weak (collective) pinning: $I_c \propto \exp(-W/T)$. Thus, in the case of weak pinning, $\ln I_c \propto 1/E^a T$. When there is strong pinning caused by local CDW deformation [23] (see Fig. 2), we must sum the contributions from strong and weak pinning, with the result that the function determining the creep rate becomes more complicated [25, 32].

Low-temperature CDW creep was first studied in thin samples of TaS_3 [30]. At temperatures above 10 K activation dependences of conductivity were registered, with the activation energy depending on the electric field, while lowering the temperature still further brought on a temperature-independent nonlinear conductivity described by the $I_c \propto \exp[-(E_0/E)^2]$ law, which is a reflection of quantum CDW creep [33–36]. Further experiments showed that a similar behavior is observed in high-quality bulk samples of TaS_3 with a low impurity concentration [37]. For this reason, quantum CDW creep as a finite-size effect is not considered in the present review.

The $NbSe_3$ compound may also exhibit CDW creep despite its metallic conduction, which is provided by uncondensed electrons and which shunts the very small contribution of the slowly moving CDW to current transfer. This was demonstrated in the experiments conducted by Thorne's group [38], in which the creep rate was measured by the narrow-band generation frequency. Such an observation is a remarkable fact since, instead of the chaotic motion expected for processes in which pinning barriers are surmounted in an activation-type manner, one observes ordered CDW motion accompanied by generation of narrow-band noise with fairly narrow spectral lines. A phenomenological model describing the speed of CDW motion as a function of the electric field was proposed by Gill [32].

2.4 A semiconductor model of a deformed CDW

At temperatures below the Peierls transition the properties of a quasi-one-dimensional conductor with complete dielectrization of the energy spectrum (the case of TaS_3) and a CDW at rest are in many respects similar to those of an ordinary semiconductor with the doping level depending on the impurity concentration [15, 19, 39–41]. A change in the length of the wave vector by δq corresponds to a relative change in the CDW charge density (i.e., a change in the doping level) by $\delta q/q$. Due to electroneutrality, this leads to the violation of the balance between the thermal excitations through the Peierls gap and, hence, to a change in the value of the linear conductivity ensured by these excitations. Since at low temperatures there are very few electrons and holes, even a small change in the length of the CDW wave vector (equivalent to doping) can bring about a considerable change in conductivity.

The electroneutrality condition can be written in the form

$$en_e \frac{q - q_0}{q_0} + eN_n \exp\left(-\frac{\Delta - \zeta}{T}\right) = eN_p \exp\left(-\frac{\Delta + \zeta}{T}\right), \tag{8}$$

where e is the elementary charge, n_e the concentration of electrons in the metallic state, q_0 the size of the CDW wave vector corresponding to this concentration, N_n and N_p the effective densities of electron and hole states, Δ the Peierls gap, and ζ the level of the chemical potential measured from the middle of the gap. The conductivity is given by the equation

$$\sigma = e\mu_n N_n \exp\left(-\frac{\Delta - \zeta}{T}\right) + e\mu_p N_p \exp\left(-\frac{\Delta + \zeta}{T}\right), \tag{9}$$

where μ_n and μ_p are the electron and hole mobilities. Assuming, for the sake of simplicity, that $N_n = N_p = N$ and $\mu_n = \mu_p = \mu$ and combining equations (8) and (9), we get

$$\sigma = en_e \mu \frac{q - q_0}{q_0} \coth\left(-\frac{\zeta}{T}\right), \tag{10}$$

where the function $\zeta(q)$ can be found by solving equation (8), which yields

$$\frac{q - q_0}{q_0} = \frac{N}{n_e} \exp\left(-\frac{\Delta}{T}\right) \sinh\frac{\zeta}{T}.$$

We see that the sensitivity of the chemical potential level to the CDW deformation rapidly increases as the temperature gets lower. For instance, in the typical quasi-one-dimensional semiconductor TaS_3 at 100 K the relative CDW deformation $\delta q/q_0 \sim 10^{-4}$, which corresponds to the occurrence of a new period of the CDW in the sample with a wavelength of about 10 μm, leads to $\zeta/T \sim 0.1$, which has an appreciable effect on

the linear conductivity, the thermoelectric coefficient, and other kinetic coefficients [40, 41] (see Section 3.8). A thorough study of the semiconductor model can be found in Ref. [19], while an example of how this model is used to quantitatively describe the jumps in the electrical resistance of TaS_3 is given in Section 3.8.1

2.5 Defects of CDWs

As in an ordinary crystal, in a uniaxial electron crystal such as a CDW there can be various defects, namely, edge and screw dislocations [11, 42] and point defects (amplitude and phase solitons) [43, 44]. These defects play an important role in CDW kinetics. Among other effects, they lead to CDW phase slip (a breaking of the CDW), which occurs near current contacts during the sliding of the CDW [45–49], and the relaxation of metastable CDW states that appear when the temperature changes. A study of the defects of CDW from the viewpoint of dislocation theory can be found in the paper by Feinberg and Friedel [42]. Note that the temperature-dependent screening of the CDW deformation results in a strong temperature dependence of the energy and size of solitons [15, 39, 50].

2.6 CDW phase slip

The very fact that the CDW kinetics and the kinetics of quasiparticles depend on different potentials leads to specific contact phenomena. Consider, for example, the distribution of potentials between two current contacts in a quasi-one-dimensional conductor without impurities. Applying a voltage across the current contacts leads to CDW sliding. This sliding results in an increase in the CDW deformation near the contacts and the occurrence of shifts in the chemical-potential level. The sliding of the CDW will continue until the difference in the electrostatic potentials between the contacts reaches zero. Since, at the same time, the difference in the electrochemical potentials remains unchanged, even in the absence of impurities the voltage applied to the sample can no more cause the CDW to slide. The increase in the CDW deformation is limited by the value at which the CDW order parameter becomes suppressed. Attempts to create a larger deformation result in the Peierls gap vanishing and in the creation (or annihilation) of a new CDW period, which reduces the absolute value of the CDW deformation. Hence, if the potential difference between the current contacts exceeds a critical value V_{ps}, steady-state sliding of the CDW emerges, and this sliding is accompanied by the periodic suppression of the order parameter, or CDW phase slip.

For a real quasi-one-dimensional conductor of length l, the threshold voltage V_T can be written in the form

$$V_T = E_T l + V_{ps}\,, \tag{11}$$

where the first term on the right-hand side describes CDW pinning, and the second term is the CDW phase slip voltage, a concept first introduced by Gill [51]. This equation is widely used when the phase slip voltage is determined from experiments. Note that in the one-dimensional case at fairly low temperatures, the phase slip voltage should be about 2Δ [47], i.e., hundreds of millivolts, but actually it only reaches values amounting to several millivolts.

Several mechanisms of CDW phase slip have been proposed. In the dislocation mechanism of Ong et al. [45], the CDW is considered as an elastic medium in which different types of dislocation are possible. Phase slip occurs because a dislocation loop formed by an edge dislocation is created [48]. An important feature of quasi-one-dimensional conductors is the possibility of new CDW periods being created from 'vacuum' at the expense of quasiparticles, while in real crystals, the growth of dislocations requires that atoms forming the crystal lattice be displaced. The gain in the elastic energy due to the creation of a dislocation loop of radius r in a charge-density wave with tension Σ amounts to $\pi r^2\Sigma$, while the energy loss is proportional to the length of the edge dislocation and is equal to $2\pi r F_d$, where F_d is the free-energy density of the edge dislocation per unit dislocation length. The total energy has a maximum, which is attained at the critical loop radius $r_c = F_d/\Sigma$ and corresponds to an energy $\pi F_d^2/\Sigma$ that determines the height of the energy barrier for the creation of an edge dislocation. If we assume that this barrier can be surmounted via thermal fluctuations, the CDW current I_c proves to be proportional to $\exp(-V_0/V_{ps})$ [48], where V_0 is a temperature-dependent parameter, and V_{ps} is the phase slip voltage measured in experiments, $V_{ps} \propto \Sigma$, $V_0/V_{ps} = \pi F_d^2/(\Sigma T)$. Ramakrishna et al. [52] derived similar equations for the probability of phase slip by using the analogy between phase slip and vortex creation in a superfluid liquid. Their model provides a satisfactory description of the shape of $I_c(V_{ps})$ for $NbSe_3$ [53], but yields excessive values for V_0 near the Peierls transition point [53]. Agreement can probably be improved by allowing for the temperature dependence of F_d, which appears because of the large contribution of the entropy term to the free energy, $F_d = W_d - TS_d$, and by assuming that three-dimensional order is destroyed because of thermal dislocation multiplication [42, 54], i.e., by assuming that $W_d - T_P S_d = 0$. Here, W_d and S_d denote, respectively, the free energy and the entropy per unit dislocation length.

The above phase slip model [48, 52] cannot be used to describe the conversion from electron current to CDW current in TaS_3, where at temperatures below 100 K the additional voltage V_{ps} becomes polarity-dependent and increases with decreasing temperature, reaching values of about 1 V [55]. The study of the potential's distribution along the sample has shown that in TaS_3, at sufficiently low temperatures the region in which electron current is converted into CDW current is rather large and extends to distances on the order of 1 mm [56]. Analysis of the experimental data for $NbSe_3$ has shown that in this compound the phase slip also occurs not only within the narrow region surrounding the current contact but far from the contact as well [57]. For this reason, Gill [57] proposed another mechanism by which CDW phase slip voltage is generated. In this mechanism, the principal contribution to V_{ps} is associated with a decrease in the collective CDW current in a large region of current conversion rather than with the CDW deformations needed for such a conversion.

A similar idea was put forward by Brazovskii and Matveenko [44, 49]. They proposed examining the following multistage current-conversion process: the injection of an electron into a quasi-one-dimensional conductor, the formation of an amplitude soliton, and the aggregation of solitons accompanied by the creation and growth of dislocation loops, which finally leads to the creation of new CDW periods.

In addition to the activation mechanism, quantum tunneling was also examined (see Refs [33–36]) as a possible mechanism of CDW phase slip. The quantum action was found to be $S_E \propto (\Sigma_0/\Sigma)^2$, where Σ_0 depends on the parameters of the quasi-one-dimensional conductor. It was

assumed [33–36] that the quantum CDW phase slip is the cause of quantum CDW creep, i.e., the occurrence, at sufficiently low temperatures, of nonlinear current–voltage characteristics that are temperature-independent and are given by the expression $I = I_0 \exp[-(E_0/E)^2]$ [30].

2.7 Metastable CDW states

The ability of CDWs to be deformed and the presence of energy barriers for both changes of configuration (CDW pinning) and changes in the mean value of the wave vector (phase slip) lead to the rise of long-lived metastable states. The existence of such states is a general property of quasi-one-dimensional conductors with CDWs [1]. Metastable states manifest themselves in the presence of temperature hystereses in conductivity [13] and the thermal emf [58]. This leads to prolonged conservation of CDW polarization after the application of an electric field above the threshold value [59] and other similar effects. The relaxation of electrical resistance in the metastable state obeys the logarithmic law $R(t)/R(t_0) = 1 + a \ln t/t_0$ [51, 59], where the relaxation rate a depends on the temperature and reaches its maximum value at $T \approx T_P/2$ in both TaS_3 [60] and $NbSe_3$ [61].

Two types of metastable states should be distinguished: metastable states related to the redistribution of the CDW phase along chains with the mean value of the wave vector retained (e.g., due to the application of an electric field), and those related to the deviation of the mean value of the wave vector from the equilibrium value (e.g., metastability caused by temperature variations). Accordingly, the mechanisms of relaxation of metastable states also differ: while the longitudinal redistribution of the CDW phase can change because of creep, phase slip is the only mechanism by which the mean value of the CDW wave vector can change. Experiments have shown that the CDW polarization relaxation can occur due to both the CDW phase slip [51] and the CDW creep [62]. The situation gets more complicated when the metastable CDW states are caused by temperature variations. The variation of the mean value of the CDW wave vector occurs because of the CDW phase slip. In sufficiently thin and short samples the elementary acts of phase slip manifest themselves as sudden changes in the electrical resistance [41]. It is obvious, however, that the nucleation of a new CDW period or the annihilation of an already existing period means that the distribution of the CDW phase within the bulk of the sample changes, i.e., the CDW phase slip is accompanied by the CDW creep. Such changes in the CDW configuration occur over distances on the order of 10 μm [29]. *A priori*, it is unclear which of the two processes (the creep or the slip of the CDW phase) determines the relaxation rate of the CDW wave vector. Experiments [60, 61] have shown that at comparatively high temperatures, $T > T_P/2$, the relaxation rate is independent of the electric field and, hence, is determined by the phase slip mechanism. At lower temperatures, when the threshold field increases, the electric field has an effect on the relaxation rate, i.e., pinning affects the relaxation processes [60, 61].

3. Finite-size effects

3.1 Regions of finite-size effects

Let us denote the phase-correlation lengths in a quasi-one-dimensional conductor by $L_\parallel^{\text{bulk}}$ and $L_\perp^{\text{bulk}}$ for directions, respectively, along and perpendicular to the chains (we assume for the sake of simplicity that the quasi-one-dimensional conductor is isotropic in the plane perpendicular to the chains). If the sample length l is smaller than $L_\parallel^{\text{bulk}}$, the CDW pinning proves to be two-dimensional and the correlation length in the perpendicular direction, $L_\perp$, for $L_\parallel < L_\parallel^{\text{bulk}}$ proves to be dependent on l. On the other hand, if the transverse dimensions of the sample, d (assumed equal), prove to be smaller than $L_\perp^{\text{bulk}}$, then $L_\parallel$ decreases. The functions $L_\parallel(d)$ and $L_\perp(l)$ can be estimated by using equation (1):

$$L_\parallel(d) \sim \left(\frac{K^2}{w_i^2 n_i}\right)^{1/3} d^{2/3}, \tag{12}$$

$$L_\perp(l) \sim \left(\frac{K^2}{w_i^2 n_i}\right)^{1/2} l^{1/2}. \tag{13}$$

Since $L_\perp(L_\parallel)$ and $L_\parallel(L_\perp)$ correspond to the bulk values of the correlation lengths, equations (12) and (13) can be written as

$$L_\parallel(d) \approx L_\parallel^{\text{bulk}} \left(\frac{d}{L_\perp^{\text{bulk}}}\right)^{2/3}, \tag{14}$$

$$L_\perp(l) \approx L_\perp^{\text{bulk}} \left(\frac{l}{L_\parallel^{\text{bulk}}}\right)^{1/2}. \tag{15}$$

To determine the dimensionality of the CDW pinning in a sample of finite dimensions via equations (12) and (13), we must know the values of $L_\parallel^{\text{bulk}}$ and $L_\perp^{\text{bulk}}$. The correlation lengths in the TaS_3 compound can be estimated from the characteristic value of the cross section of the onset of finite-size effects, $L_\perp^{\text{bulk}} \sim 1$ μm [41], and from the characteristic length over which the CDW configuration changes as a result of relaxation of metastable states, $L_\parallel^{\text{bulk}} \sim 10$ μm [29]. Direct measurements of correlation lengths done for $NbSe_3$ by the X-ray diffraction method [28] gave $L_\parallel = 0.9$ μm, $L_\perp = 0.1$ μm for impure samples ($R(300\text{ K})/R(4.2\text{ K}) = 10$) and $L_\parallel > 2.5$ μm, $L_\perp > 1.9$ μm for clean samples ($R(300\text{ K})/R(4.2\text{ K}) = 300$). Figure 3 shows the expected dimensionality of the CDW pinning as a function of the sample size for a quasi-one-dimensional conductor with $L_\parallel^{\text{bulk}} = 10$ μm and $L_\perp^{\text{bulk}} = 1$ μm, where for the sake of simplicity the transverse dimensions of the sample are assumed equal. A reduction in the sample length to $l < L_\parallel$ lowers the pinning dimensionality from three to two, with $L_\perp$ decreasing in accordance with (15). Similarly, a reduction in the diameter of a long sample to a value smaller than $L_\perp$ lowers the pinning dimensionality to unity, while $L_\parallel$ decreases according to (14). When all dimensions of the sample are smaller than the respective correlation lengths, pinning becomes zero-dimensional.

3.2 Technological means of fabricating small-size samples

3.2.1 Selection of small samples from a growth batch. A direct way to fabricate small samples is to select thin samples from a growth batch and then place them on a substrate to fabricate contacts needed for measurements. This method was widely used to study finite-size effects in $NbSe_3$ [3, 18, 61, 63]. Samples fabricated in this manner are the most perfect ones and contain the smallest number of defects compared to samples fabricated by other methods, which are described in Sections 3.2.2–3.2.6. However, this method places important restrictions on the minimum size of the sample: only samples with a thickness not smaller than 0.05 μm and width on the order of 1 μm can be fabricated by this method.

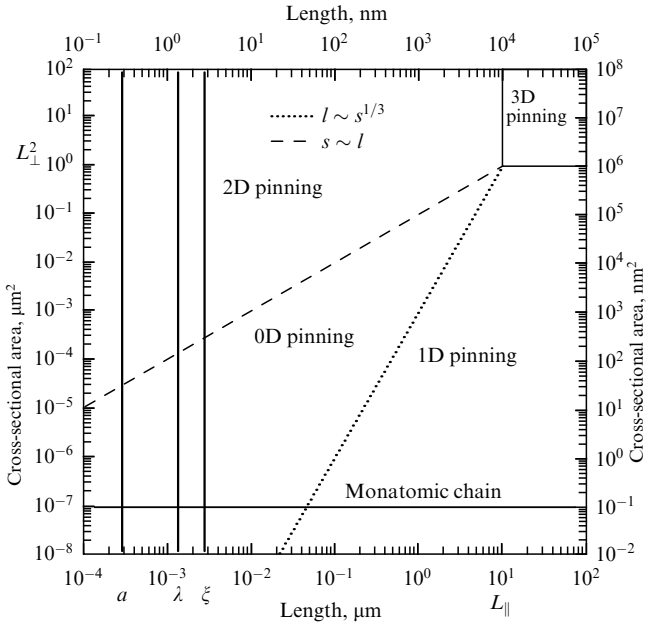

Figure 3. Dimensionality of the CDW pinning as a function of the sample dimensions for a quasi-one-dimensional conductor with $L_\parallel^{\text{bulk}} \sim 10$ μm, $L_\perp^{\text{bulk}} \sim 1$ μm, and $\lambda = 2\pi/q$.

3.2.2 Sample splitting. Quasi-one-dimensional conductors are filamentary crystals with highly anisotropic properties. The high anisotropy makes it possible to split quasi-one-dimensional conductors into very thin filamentary samples whose cross-sectional area may amount to less than 10^{-3} μm^2.

In this method a fairly thick sample of TaS_3 is placed on a precleaned substrate made of fused silica or sapphire. Then, one end of the sample is split with a specially sharpened needle and the sample is separated into several thinner samples. The thinnest samples are attracted to the substrate so strongly that they cannot be moved without damaging them. The large samples are removed from the substrate by a strong jet of air. The most perfect samples among the remaining thin ones are provided with contacts and used for further studies. This method is widely used to fabricate samples with cross-sectional areas reaching 10^{-3} μm^2. Most finite-size effects in TaS_3 [30, 41, 64 – 69] were discovered in samples fabricated by the splitting method.

3.2.3 Thin films of quasi-one-dimensional conductors. Because of the high anisotropy of the crystal structure it is extremely difficult to fabricate high-quality thin films of quasi-one-dimensional conductors, and the first reports about growing still imperfect mosaic films of $Rb_{0.3}MoO_3$ by laser ablation [70, 71] appeared rather recently. The development of this method by a group from Technische Univ. Delft became a new important step in the development of technologies used to fabricate quasi-one-dimensional conductors. Unfortunately, the polycrystallinity of the structure of the fabricated films and the large number of defects make such films considerably less interesting compared to thin split single-crystal plates of quasi-one-dimensional conductors. Today, this method is almost never used.

3.2.4 Ultrasonic dispersion. According to a recent report [72], a new promising method of fabricating small crystals of quasi-one-dimensional conductors has been developed. It is based on splitting quasi-one-dimensional conductors with ultrasound. A 'solvent' is applied to the quasi-one-dimensional conductor that is to be dispersed, and the system is placed in an ultrasonic bath. Ultrasonic treatment produces a suspension of thin crystals of the quasi-one-dimensional conductor, with the characteristic dimensions of the crystal depending on the intensity of the ultrasound and the duration of treatment. A drop of such a suspension can be placed on almost any substrate. After it dries out, crystals remain on the substrate, and these can be used in further measurements. For the 'solvent' one can take a surfactant that prevents the dispersed crystals from sticking together. This method makes it possible to easily split such quasi-one-dimensional conductors as TaS_3, NbS_3, $TaSe_3$, and $NbSe_3$. Among the drawbacks of this method is the impossibility of fabricating samples with large length-to-thickness ratios and the possibility of reactions occurring between the 'solvent' and the quasi-one-dimensional conductor.

3.2.5 Splitting by electric field. This is a very new method developed for the fabrication of thin samples [73]. It consists of applying a potential $V \approx 20$ kV to a relatively thin sample of a quasi-one-dimensional conductor placed in a vacuum. The strength of the electric field generated at the surface of a sample with a diameter d of about 1 μm proves to be on the order of $2V/d \approx 40$ V nm^{-1}, i.e., on the order of the interatomic field. This 'fluffs' the sample into long filaments. The thinnest TaS_3 and $NbSe_3$ samples have been fabricated in just this way [74].

3.2.6 Fabricating mesoscopic structures and the thinning of samples. Modern technoloqies make it possible to create complicated structures of micrometer dimensions. For instance, electron-beam lithography can produce an image of the future structure on the surface of a resist-covered sample. The areas on the surface not protected by the resist can be removed by reactive etching in SF_6 plasma. Such structures can also be fabricated via etching with a focused ion beam. These methods have great potential in fabricating relatively large structures based on quasi-one-dimensional conductors [5, 75]. Since the initial sample must have micrometer dimensions and etching damages the surface layer of the sample to a depth of about 20 nm, the above methods cannot be used to fabricate structures with dimensions smaller than 50 nm [5]. A detailed description of these methods, together with examples of their application, can be found in Refs [5, 75]. Reactive plasmochemical etching has been successfully used in the studies of finite-size effects to make $NbSe_3$ samples thinner [76], while the method of etching by a focused ion beam has been used to reduce the width of the samples [75, 77].

In addition, the thinning of samples can be done by oxidizing the surface (under natural conditions or at an elevated temperature). Slow oxidation of the surface of quasi-one-dimensional conductors was discovered fairly recently [72, 74] and requires further study.

3.3 Manifestations of finite-size effects

As noted in Section 3.1, in quasi-one-dimensional conductors with CDWs, the phase correlation length in the direction perpendicular to the chains is on the order of 1 μm. This means that for samples whose transverse dimensions are much smaller than 1 μm, pinning may be considered one-dimensional, and many properties of quasi-one-dimensional

conductors prove to be dependent on size. It has been demonstrated that the dimensions of samples greatly affect almost all physical characteristics of quasi-one-dimensional conductors with CDWs. The list of finite-size effects includes the following observations: dependence of the narrow-band noise spectral width [41], the quantities E_T [3, 41, 63] and T_P [26, 41], the high-frequency conductivity [3], and the relaxation rate of metastable states [61] on the transverse sizes of the samples; jumps in the resistance of thin samples [41]; the smearing of the threshold field in the current–voltage characteristics of thin samples [3, 26]; the onset of threshold conductivity at $T > T_P$ [68]; mesoscopic oscillations of the threshold field [66]; transition to one-dimensional conduction as the transverse dimensions of the samples diminish [76]; quantum CDW creep [30]; absolute negative resistance of quasi-one-dimensional conductors [18]; dependence of the CDW phase slip voltage on the distance between the current contacts [78]; and the Aharonov–Bohm effect in CDW sliding [79]. These effects are discussed in detail in Sections 3.4–3.15.

3.4 Dependence of threshold field on the sample thickness

The dependence of the threshold field for the nonlinear conduction on the transverse dimensions of samples was one of the first finite-size effects observed. Figure 4 depicts the dependence of the nonlinear-conduction threshold field on the cross-sectional area s of TaS_3 samples. Clearly, as the cross sectional area decreases from 100 μm^2 to 10^{-2} μm^2, the nonlinear-conduction threshold field increases by more than 1.5 orders of magnitude. An increase in the threshold field accompanying the decrease in the sample thickness has also been observed in $NbSe_3$ [3, 63], where it has been found that $E_T \propto s^{-1/2}$.

Two models that explain this increase in the threshold field have been proposed. In the first (earlier) model it was assumed that the effect is a result of the CDW pinning by the crystal's surface, since the ratio of the sample's surface area to the volume is proportional to $s^{-1/2}$. This point of view was also supported by Gill's group [63, 80]. In an alternative explanation put forward by Thorne's group [3, 81] it was assumed that there is a dependence of the threshold field on the transverse dimensions of the samples within the framework of the weak pinning model [see equations (2) and (3)]. A detailed analysis of the dependence of the threshold field on the impurity concentration and the sample dimensions has led the authors of Refs [3, 81] to the conclusion that it is precisely weak two-dimensional CDW pinning that is responsible for the increase in the threshold field in $NbSe_3$ according to the $E_T \propto s^{-1/2}$ law [2].

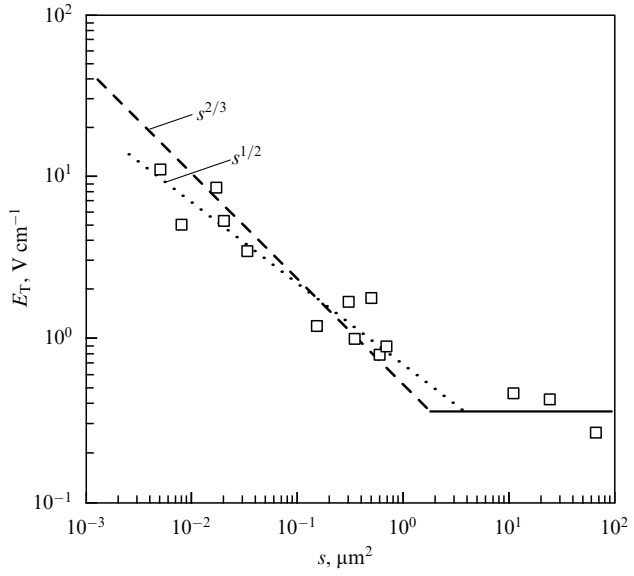

Figure 4. Dependence of the nonlinear conduction threshold field on the cross-sectional area of TaS_3 samples at $T = 120$ K. (Data taken from Ref. [41]).

In contrast to the properties of $NbSe_3$, which has a layer structure, the properties of TaS_3 in the directions perpendicular to the metallic chains are very similar, and in thin samples of this compound one should expect a transition to one-dimensional pinning. In this case, the analysis of the weak pinning model [see equation (2)] produces the dependence $E_T \propto s^{-2/3}$, which also agrees with the experimental data, just as the dependence $E_T \propto s^{-1/2}$ does (see Fig. 4). Thus, for TaS_3 the analysis of the function $E_T(s)$ does not allow us to distinguish between the different manifestations of the possible effects described above. The way to resolve this problem is discussed in Section 3.10, which is devoted to the mesoscopic fluctuations of the threshold field [66]. There, we show that in short, thin TaS_3 samples zero-dimensional CDW pinning is realized. This means that the increase in the threshold field in TaS_3 samples corresponds to zero-dimensional CDW pinning with $E_T \propto s^{-2/3}$.

3.5 Dependence of AC conductivity on transverse dimensions of samples

Figure 5 shows the frequency dependencies of the imaginary part of the linear conductivity for three $NbSe_3$ crystals of different thicknesses. On the whole, the measured curves agree with the predictions of equation (5) (shown by dots).

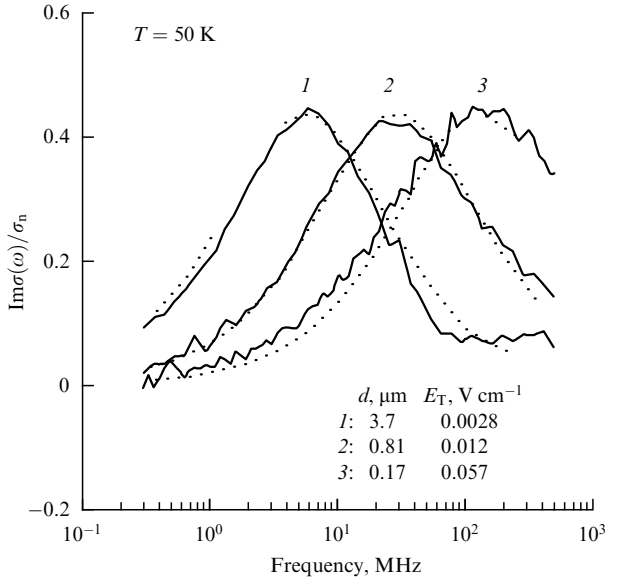

Figure 5. Frequency dependencies of the imaginary part of AC conductivity for thin pure samples of $NbSe_3$ at $T = 50$ K. The dots are the results of data fitting by equation (5). The sample thickness and the threshold field are indicated in the figure.

[2] More specifically, the authors of Ref. [3] concluded that $E_T \propto 1/d_\perp$, where $d_\perp$ is the sample thickness ($d_\perp \ll L_\perp$).

Clearly, there is a distinct dependence of the characteristic frequency ω_0 on the dimensions of the sample, with this frequency being proportional to the threshold field E_T, as expected (see equation (6)). The data are described satisfactorily by the superposition of the curves predicted by equation (5), with a Lorentzian distribution of the characteristic frequencies ω_0.

3.6 Finite-size effects near the phase transition temperature

3.6.1 Dependence of the phase transition temperature on the transverse dimensions of the samples. The characteristic features of quasi-one-dimensional conductors are the large width of the Peierls transition and the broad region of fluctuational conduction near the transition. At temperatures $T > T_P$ fluctuation traces of the Peierls state can be observed through optical measurements [82], X-ray diffraction studies [83, 84], and investigation of the linear and nonlinear conduction of quasi-one-dimensional conductors [85].

Figure 6 shows $d\ln R/d(1/T)$ for TaS_3 samples of different thicknesses as a function of the reciprocal temperature $1/T$. Clearly, as the transverse dimensions of the samples diminish, there appears a distinct shift of the transition toward lower temperatures and the transition spreads out.

The broadening of the Peierls transition and its shift toward lower temperatures as the samples get thinner was also observed in other quasi-one-dimensional conductors, e.g., in $NbSe_3$ [3, 26], and in $Rb_{0.3}MoO_3$ films [71]. Thus, the dependence of the shape and temperature of the Peierls transition on the transverse dimensions of the samples is a general property of quasi-one-dimensional conductors with CDWs.

3.6.2 Smearing of the threshold field in thin samples at temperatures $T < T_P$. Nonlinear conduction in bulk samples of quasi-one-dimensional conductors occurs in a comparatively narrow range of electric field and is characterized by a well-defined value of the threshold field. McCarten et al. [3] and Gill [26] reported a dramatic change in the nature of the nonlinear conduction in thin $NbSe_3$ samples, namely, the disappearance of a threshold and occurrence of smooth current – voltage characteristics. Figure 7 shows a typical set of curves representing the differential resistance dV/dI of a thin sample of $NbSe_3$, in which such behavior most vividly manifests itself, as a function of the electric field at different temperatures. Similar behavior is observed in thin TaS_3 samples [69].

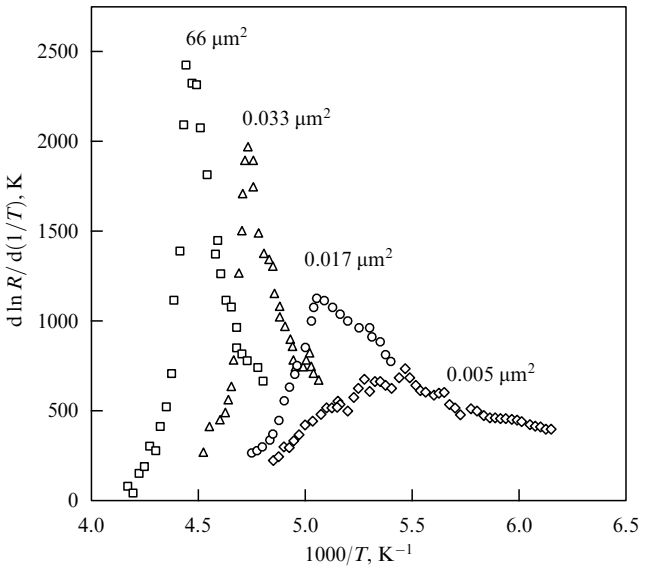

Figure 6. Dependence of $d\ln R/d(1/T)$ for thin TaS_3 samples on the reciprocal temperature near the Peierls transition. The squares correspond to the sample cross-sectional area of 0.66 μm², triangles to 0.033 μm², circles to 0.017 μm², and lozenges to 0.005 μm². (Data taken from Ref. [41].)

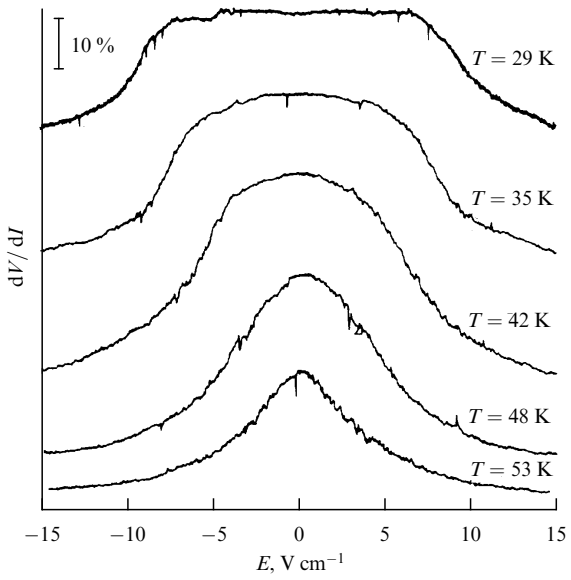

Figure 7. Differential resistance of a thin $NbSe_3$ sample as a function of the electric field near the Peierls transition point. (Data taken from Ref. [3].)

3.6.3 Occurrence of a threshold field at temperatures $T > T_P$. The occurrence of threshold nonlinear conduction in thin samples at $T > T_P$ is one of the most peculiar finite-size effects [68]. Figure 8 shows a set of curves representing the dependence of the differential resistance of a thin TaS_3 sample on the voltage across the sample near the Peierls transition point. At temperatures below T_P (Fig. 8a), the function $R_d(V)$ has its ordinary shape, with the nonlinear conduction appearing at voltages higher (in absolute value) than the threshold voltage. At temperatures near $T_P = 220$ K and higher, the current – voltage characteristic acquires an additional (quadratic in the voltage) nonlinearity, which is an indication of the fluctuational nature of CDW motion. After subtracting this quadratic nonlinearity, one obtains current-voltage characteristics that manifest the threshold behavior of the nonlinear conduction up to temperatures exceeding T_p by 45 K. Such behavior by the current – voltage characteristics can be observed in samples with the cross-sectional area on the order of 0.1 μm², where finite-size effects are still not very strong. In thinner samples the fluctuation effects, which lead to the smoothing of the current – voltage characteristics [3, 26], prove to be so strong that the fairly weak threshold nonlinearity cannot be reliably identified. This was also observed by Thorne [86] in experiments with $NbSe_3$. No threshold conduction at $T > T_P$ has been observed in bulk samples [85].

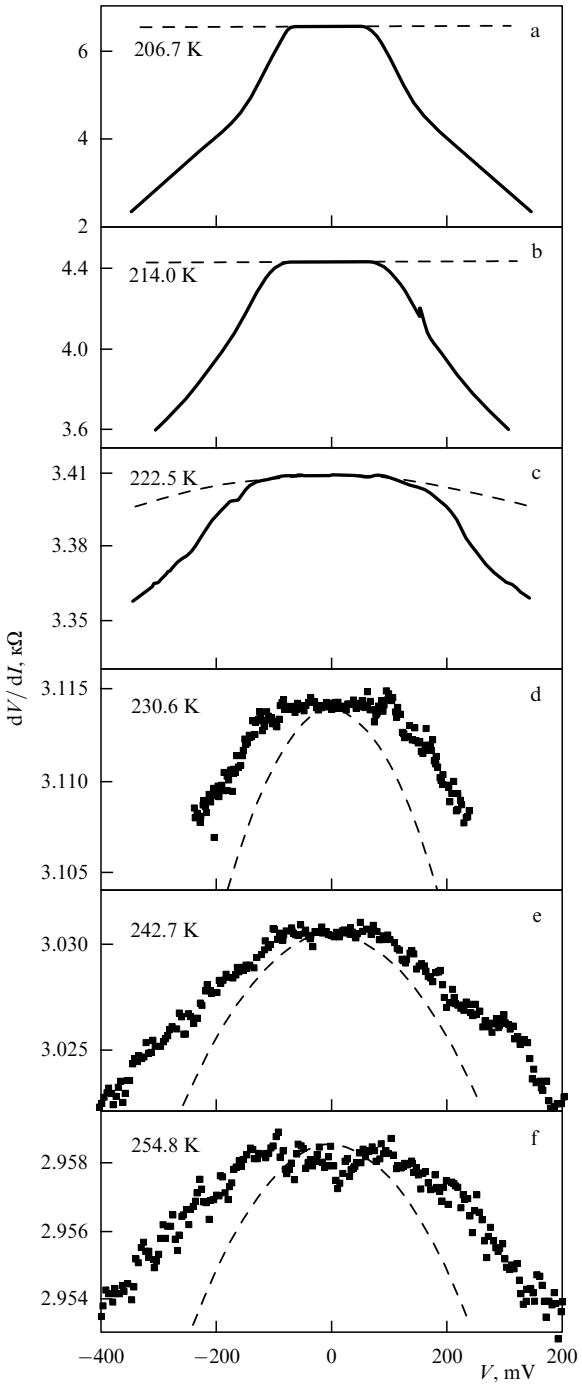

Figure 8. Differential resistance of a thin TaS_3 sample as a function of the voltage near the Peierls transition point after subtrating the smooth nonlinearity depicted by dashed curves. (Data taken from Ref. [68].)

3.6.4 Phenomenological model of the CDW behavior near the Peierls transition temperature. The problems associated with the origin of the smearing of the phase transition and the current – voltage characteristics in thin samples of quasi-one-dimensional conductors are extremely complicated. First, these effects can be related neither to the bounding of the phonon spectrum nor to the changes in the electron spectrum caused by finite-size quantization, since the characteristic energies of finite-size quantization for a sample with transverse dimensions on the order of 100 nm are much lower than the Peierls transition temperature. Most probably, these two phenomena are related to the rise in fluctuations and the drop of the pinning energy as the samples get thinner. As proposed by McCarten et al. [3] and Gill [26], who studied the properties of thin $NbSe_3$ samples, the rise in fluctuations is related to the drop of the CDW pinning energy per CDW phase correlation volume. This energy becomes so small that CDW thermal activation effects, which lead to activated CDW creep [3] or 'Brownian CDW motion' in the periodic punning potential [26], become possible. Actually, we are dealing here with phase fluctuations of a continuous CDW. Remaining within such an approach, one can estimate the excess conductivity and the characteristic value of the nonlinear-conduction threshold field for quasi-one-dimensional conductors near the phase transition point.

The quantitative estimates of the effect made in Refs [3, 26] are based on the assumption that the mean-field approximation can be used to describe the Peierls state and the Peierls transition. According to the mean-field approximation, as we move toward the Peierls transition from the low-temperature side we should expect a reduction in the order parameter that obeys a law similar to the dependence of the BCS (Bardeen – Cooper – Schrieffer) theory of superconductivity. All traces of the Peierls state should disappear at $T > T_P$ and the Peierls transition should emerge at $T_P = \Delta(0)/1.76$. It is well known, however, that for almost all Peierls conductors, in particular for $NbSe_3$, $\Delta(0)/T_P \approx 4$, and the Peierls gap (precisely, the pseudogap) occurs at temperatures that are hundreds of degrees higher than the Peierls transition temperature [82]. It is also known that the temperature dependences of the electron concentration in CDWs in the $NbSe_3$ and TaS_3 compounds are almost steplike and are poorly described by the BCS theory [83, 87]. On the other hand, it is also known that at the Peierls transition temperature there is three-dimensional ordering of CDW rather than CDW formation. For these reasons it is highly improbable that the BCS theory can be used to describe the Peierls transition and its smearing even in the case of $NbSe_3$. Deviations from the BCS theory in the case of TaS_3 are even more evident, and therefore there is even less reason to use such ideas to describe the shape of the Peierls transition and the dependence of this transition on the dimensions of the samples.

The origin of this effect, at least in TaS_3, is probably different. The effect could be related (see Ref. [68]) to fluctuations in the CDW amplitude, i.e., spontaneous CDW phase slip near the Peierls transition. Studies of the hysteresis loop in the temperature dependence of conductivity in bulk TaS_3 samples showed that metastable states disappear near T_P, i.e., the energy barrier for the spontaneous CDW phase slip disappears [88]. Thus, the Peierls transition may be caused by the destruction of three-dimensional CDW order due to CDW dislocation multiplication [42, 54, 65, 88, 89].

If we remain within the scope of these ideas, we can conclude that the change in the shape of the transition and the transition's shift toward lower temperatures in thin samples are caused by the rise in the phase slip intensity. The enhancement of the CDW phase slip in thin samples can be noticed by the narrowing of the resistance hysteresis loop [41], the occurrence of spontaneous resistance fluctuations [64, 65, 89], and the increase in the relaxation rate of metastable states [61]. The rise in fluctuations can be caused by two reasons. First, as the transverse dimensions of thin samples get

smaller, so does the correlation length, which means that nonuniform deformation of CDWs increases. On the other hand, in a sample with finite dimensions it is easier for dislocations to be created because of the decrease in the free energy per unit length of dislocation line, a situation we discuss in greater detail in Section 3.9, where we describe the finite-size effects in the relaxation of metastable states. Recent microscopic calculations [90] also suggest that there are exceptionally strong fluctuations in CDW tension, fluctuations that may suppress the order parameter near the Peierls transition. However, a theory has to be developed that would describe the shape of the resistive Peierls transition and the evolution of the transition under changes in the transverse dimensions of the samples.

Pokrovskii et al. [68] proposed a model that describes the occurrence of threshold nonlinear conduction at temperatures above the phase transition point. The model takes into account the fluctuational creation of CDW domains at $T > T_P$ and their depinning by an electric field. As the electric field grows, the characteristic sizes of the domains that contribute to nonlinear conduction diminish. The current – voltage characteristic of a sample of finite sizes consists of two regions: the initial region, where the maximum sizes of the domains contributing to the nonlinear conduction are limited by the sample's thickness, and the high-field region, where the depinning of fluctuationally born CDW domains occurs in the same way as in a bulk sample. The crossover between these two regions manifests itself as the threshold voltage in the current – voltage characteristic.

3.7 The absence of a finite-size effect in Shapiro steps as an argument in favor of bulk CDW pinning

A vivid manifestation of the periodic nature of the impurity – CDW interaction is the occurrence of Shapiro steps in the current – voltage characteristics of quasi-one-dimensional conductors [91]. This phenomenon can be observed when a combined AC-DC voltage $V(t) = V_{dc} + V_{ac} \sin \omega t$ is applied to a quasi-one-dimensional conductor. When the frequency of narrow-band noise, which begins as a result of CDW sliding, coincides with the frequency of the applied external AC signal, a step appears in the current – voltage characteristic; namely, the nonlinear current ceases to depend on the voltage when the latter is varied within a certain range δV. The dependence of the step's width on the amplitude V_{ac} of the alternating voltage has oscillatory shape and is described by Bessel functions. Similar phenomena are observed at multiple frequencies. The dependence of the relative width of the first step, $\delta V/V$ (coincidence of frequencies), on the transverse dimensions of $NbSe_3$ samples has been studied by McCarten et al. [3]. The researchers detected no dependence of the step width on the cross section area. Such a behavior, according to their conclusion, indicated that the mechanisms of pinning in bulk and in thin $NbSe_3$ samples coincide, i.e., surface pinning provides no significant contribution.

3.8 Jumps in the CDW configuration in thin TaS_3 samples

3.8.1 Jumps in resistance. The first experiments with thin TaS_3 samples [41] revealed stepwise changes in the temperature dependence of linear resistance. Figure 9 shows the temperature dependence of the resistance of a thin TaS_3 sample. The most important and new feature of this temperature dependence is its stepwise structure. The inset in Fig. 9 depicts a fragment of the $R(T)$ function for a thin sample subjected to

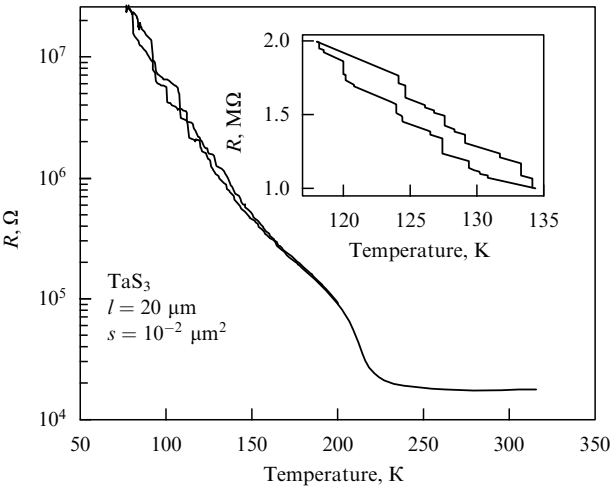

Figure 9. Temperature dependence of the resistance of a small TaS_3 sample. The inset depicts a fragment of the $R(T)$ dependence under thermal cycling in the 118 – 134-K range.

thermal cycling in the 118 – 134 K temperature interval. A hysteresis loop is clearly visible, and the dependence $R(T)$ consists of rectilinear sections in which the activation energy $\mathrm{d} \ln R/\mathrm{d}(1/T) \approx 200$ K is approximately four times lower than the average conduction activation energy $\Delta = 800$ K. The transition from one section to another is stepwise. The typical scale of the relative variation of the resistance amounts to 1 – 10%, and the distance between the jumps depends on the temperature and the sample's length: as the temperature increases or as the length increases, the temperature intervals between the jumps get smaller. The jumps are always directed toward the center of the hysteresis loop. The motion between neighboring jumps is reversible and is not of a hysteresis nature.

In the case of the thinnest samples with cross-sectional areas $s \ll 10^{-2}$ μm^2, the hysteresis loop gets narrower, the temperature at which hysteresis appears decreases; the jumps become smeared, and their amplitude decreases. Measurements of such smeared jumps have shown that actually in the region where a jump is smeared there is multiple switching between two or more states with different resistances, and the amount of time during which the sample stays in each of these states is temperature-dependent [64]. The inset in Fig. 10 shows a fragment of the dependence $R(T)$ measured with the temperature gradually changing in the area of the jump. Clearly, as the temperature grows, the probability of the sample being in its initial state slowly decreases, and so gradually the sample gets into a new state with a somewhat lower resistance.

The spontaneous transitions between metastable states occurring in the region of smeared jumps manifest itself in the temperature dependence of the conduction noise of a short, thin TaS_3 sample (see Fig. 10). The temperature regions where the noise intensity increases dramatically are relatively narrow, and the distance between such regions in the given sample is on the order of the region width. In longer samples the different temperature regions of increased noise from different sections of the sample overlap, and it becomes almost impossible to observe individual temperature regions of increased noise.

As noted in Section 2.1, in orthorombic TaS_3 the size of the CDW wave vector q is temperature-dependent. This

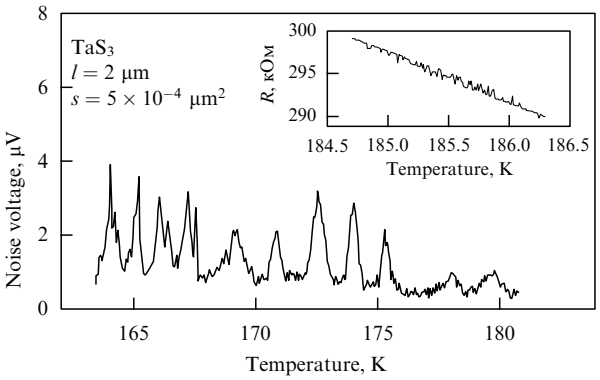

Figure 10. Temperature dependence of the noise voltage in a thin TaS_3 sample with a 2-mV mean voltage across the sample. The inset shows a fragment of the temperature dependence of the resistance of the same sample near the smooth jump in resistance. The dependence was measured with the rate of temperature increase dT/dt being 0.7 K min^{-1}.

means that the number N of CDW periods in a sample of length l, $N = l/\lambda$, where $\lambda = 2\pi/q$, depends on the temperature. In a sample of infinite length, a change in the wavevector is possible only at the expense of CDW rupture and the creation of a new period or the disappearance of an old one, i.e., at the expense of CDW phase slip. In a sample of finite length, the wave vector may also change because of the entrance (exit) of CDW periods through the ends of the sample, which changes the CDW configuration at a distance on the order of $V_{ps}/2E_T$ from the ends. Anyway, it is natural to relate the detected stepwise changes in the resistance with the creation (annihilation) of new CDW periods in the sample. Beginning with the first work devoted to the temperature hysteresis of conductivity in TaS_3 [13], this hysteresis was related to that of the Peierls gap, which emerges because of the temperature dependence of the CDW wave vector. This statement was based on the observation that the conduction activation energy depends on the direction in which the temperature changes (traces of this effect can be seen in Fig. 9). But verification of this hypothesis proved to be a difficult task since there was no data on the scale of the necessary changes in the wave vector. The data from Ref. [41] allows us to make certain estimates. For a sample of length $l \approx 20$ μm (see Fig. 9), the characteristic variation of the CDW wave vector amounts to only $\delta q = 2\pi/l \sim 10^{-4}q$, while the observed characteristic change in resistance amounts to 1–10%, i.e., is more than hundred times higher. Below, we give a quantitative explanation of such an increase in the scale of the effect and show that no ideas related to the dependence of the energy gap on the CDW wave vector are required.

The conductor TaS_3 obeys the condition $q - q_0 > 0$ [12], which according to equation (8) yields p-type conduction. This result agrees with the experimental data on thermal emf [92] and the Hall effect [93] and with the positions of the resistance equilibrium values inside the hysteresis loop [94].

Following Ref. [41], as the first approximation we take the case of unipolar conduction $\zeta \gg T$. Then equations (8) and (9) yield $\sigma = en_0\mu(q - q_0)/q_0$, and the size of the jump is given by the expression

$$\frac{\delta\sigma}{\sigma} = \frac{\sigma_0}{\sigma}\,\frac{\mu}{\mu_0}\,\frac{\lambda}{l}\,, \tag{16}$$

where the subscript '0' refers to the metallic state. Substituting the measurement data $\sigma_0/\sigma(120\ \mathrm{K}) = 100$, $\lambda/l = 10^{-4}$, and $\mu/\mu_0 = 10$ [93], we obtain $\delta\sigma/\sigma = 10\%$, which agrees with the results of experiments (see Fig. 9). What this means is that the CDW phase slip, which changes the number of the CDW periods, occurs over the entire cross section of the sample.

A more precise approach [41] consists of allowing for the asymmetry between the electron and hole states, which can be included in the reasoning as a shift of the chemical potential in the equilibrium state, $|\zeta| \sim T$. This shift can be estimated by the value of the conduction activation energy between the jumps. Indeed, the reversible regions of the dependence $\sigma(T)$ between the jumps correspond to fixed values of the CDW wave vector, and the activation energy Δ^* in these regions can be estimated as $d\ln\sigma/d(1/T)$ with q constant:

$$\Delta^* = \frac{\Delta}{\cosh^2(\zeta/T)}\,. \tag{17}$$

Using the relationship and the experimental values $\Delta^* = 200$ K and $\Delta = 800$ K, we find that $\zeta/T = -1.3$ (the 'minus' sign corresponds to the hole nature of the conduction). Note that this quantity also incorporates the differences in the effective densities of states and mobilities for electrons and holes, which means that it has no direct physical meaning, being only the measure of asymmetry of the electron and hole states.

3.8.2 Characteristic lengths of change of the CDW configuration in TaS_3. After the observation of the jumps in conductivity [41], the question emerged of how to determine the distances over which the changes in the CDW configurations occur in such jumps. The development of the semiconductor model of quasi-one-dimensional conductors has made it possible to propose a method for measuring the correlation length. The study of the spatial distribution of the CDW phase in single acts of phase slip was based on the method of investigating the CDW deformation proposed by Itkis et al. [40]. The method consists of determining the spatial distribution of the thermal emf voltage generated by the heating, with a focused laser beam, of the sample suspended between the contacts. The thermal emf $\varepsilon(x)$ generated as a result of heating the sample at a point with the coordinate x is related to the shift in the chemical potential and, therefore, to the CDW tension in the following way: $d\varepsilon(x)/dx \propto S(x) \propto \zeta(x) + \mathrm{const}$, where S is the Seebeck coefficient. Hence, by measuring the derivative $d\varepsilon(x)/dx$ we can get information about the spatial distribution of the CDW deformation.

Figure 11 shows a series of curves $S \propto d\varepsilon(x)/dx$ obtained with a spatial resolution of 1 μm under slow temperature variations in a thin TaS_3 sample [29]. Clearly, the spatial distribution of $S(x)$ is nonuniform, the nonuniformity spatial scale being on the order of 10 μm. Stepwise changes of $S(x)$ cover a distance of 10 μm. Resistance measurements carried out simultaneously revealed that to each sudden change in $S(x)$ there corresponds a jump in resistance.

Thus, the relation between the shift in the chemical potential and the CDW deformation makes it possible to measure the characteristic scale of CDW configuration variations caused by single acts of phase slip (see Fig. 11). Since the characteristic variations of the phase resulting from phase slip are equal to 2π, such variations make it possible to estimate the longitudinal length of CDW phase correlation as 10 μm. Note that determining the correlation length of such a

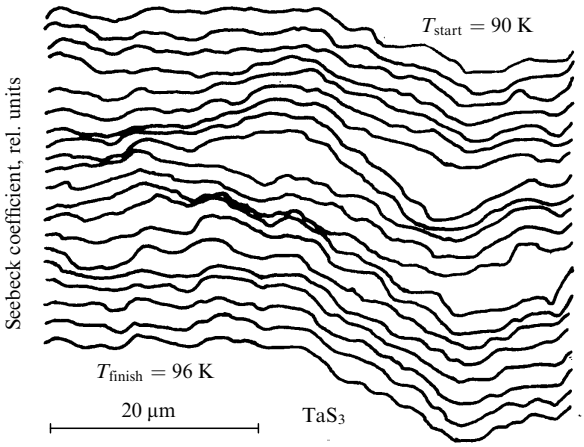

Figure 11. Temperature evolution of the spatial distribution of the Seebeck coefficient. For pictorial reasons, the curves obtained under smooth temperature variations are shifted vertically. (Data taken from Ref. [29].)

magnitude by direct X-ray diffraction methods is very difficult (if possible at all).

3.9 Effect of the transverse dimensions of samples on the relaxation rate of metastable states

The narrowing of the conduction hysteresis loop in TaS_3 crystals of small transverse size [41] mentioned in Section 3.8.1 and the direct measurements of the logarithmic relaxation rate in $NbSe_3$ [61] suggest that the decrease in the transverse dimensions of quasi-one-dimensional conductors leads to the acceleration of the relaxation of metastable CDW states. In sufficiently thin samples with a cross-sectional area on the order of 10^{-3} μm^2, hysteresis practically disappears, and spontaneous conductivity fluctuations emerge, which indicates that there are spontaneous variations in the CDW wave vector, i.e., spontaneous CDW phase slip [64, 65].

All these observations suggest that there is a finite-size effect in the CDW phase slip and that this effect is responsible for the relaxation of metastable states. There are two reasons why spontaneous phase slip is facilitated in thin samples of one-dimensional conductors. First, the correlation length diminishes because of the finite-size effect. This decrease leads to an increase in the nonuniform deformation of the CDW, which, in turn, lowers the barrier for phase slip. Second, within the dislocation [11, 42] and vortex [48] approaches to topological defects in CDWs, the energy of a unit dislocation length in a sample of infinite sizes, W_d, is proportional to $\ln \xi/\xi_0$, where ξ is the characteristic spatial scale of the perturbation generated by the dislocation, and ξ_0 is the amplitude CDW correlation length, $\xi_0 = v_F/\Delta \sim 3$ nm. In such a sample, ξ coincides with the phase correlation length, while in small samples this length is limited by the sample's sizes. As ξ decreases from 3 μm in a bulk sample to 100 nm in a thin sample, the dislocation energy at zero temperature decreases twofold, which facilitates the creation of dislocations and speeds up the relaxation of metastable states. At a finite temperature, the decrease in energy is even more noticeable because of the presence of the entropy term in the dislocation's free energy.

3.10 Mesoscopic oscillations of the threshold field

Studies of the temperature dependence of the threshold field for the CDW sliding [66] in short, thin TaS_3 samples have revealed that in such samples there emerge aperiodic variations of the threshold field with the relative value of about 0.1 – 0.2 of its mean value, irrespective of the number of impurities in the samples. Such behavior results from the fact that zero-dimensional CDW pinning has been achieved in the samples under investigation and can be placed in the class of mesoscopic phenomena, i.e., phenomena that emerge in physical objects that consist of a large number of atoms but have dimensions much smaller than the characteristic lengths [95]. The characteristic scales of variation of the threshold field indicate the presence of mixed pinning, which was proposed by Abe [23].

Figure 12 shows a fragment of the temperature dependence of the threshold voltage of a short, thin TaS_3 sample [66]. Clearly, the dependence $V_T(T)$ experiences substantial irregular variations, and the scale of these variations is much larger than the error in determining V_T (< 2%).

For the measure of the scale of fluctuations of V_T we took the root-mean-square deviation $\delta V_T = [\langle (V_T - V_T^*(T))^2 \rangle]^{1/2}$ from the function $V_T^*(T)$, obtained by approximating the function $V_T(T)$ in the temperature interval from 120 to 180 K by polynomials of the third or fifth degrees. The dependence of $\delta V_T/V_T$ on the sample length is depicted in Fig. 13. The characteristic value of the rms fluctuations in the threshold field was found to increase 10% for samples whose length is on the order of 10 μm to 20% for samples whose length is on the order of 1 μm.

The origin of the threshold field fluctuations is similar to that of conductivity fluctuations in mesoscopic samples of metals. The temperature dependence of the CDW wave vector in TaS_3 determines the temperature dependence of the CDW configuration that is in equilibrium with respect to the pinning centers.

In the strong pinning limit, where the phase is pinned by each impurity independently and the role of CDW elasticity is negligible, the threshold field cannot depend on the equilibrium CDW configuration. Thus, the case of strong pinning does not agree with the observed behavior.

If the threshold field appears as a result of weak pinning, then we can expect that at least in the shortest samples the CDW is coherent along all directions, i.e., CDW pinning in such samples is zero-dimensional. In the case of zero-

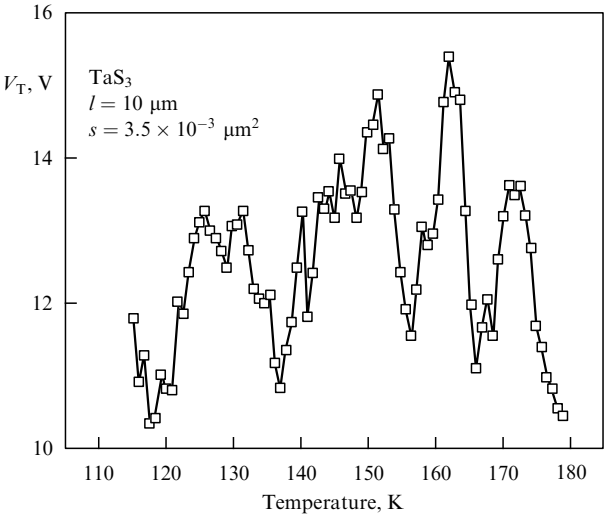

Figure 12. Fragment of the temperature dependence of the threshold field for a small TaS_3 sample. (Data taken from Ref. [66].)

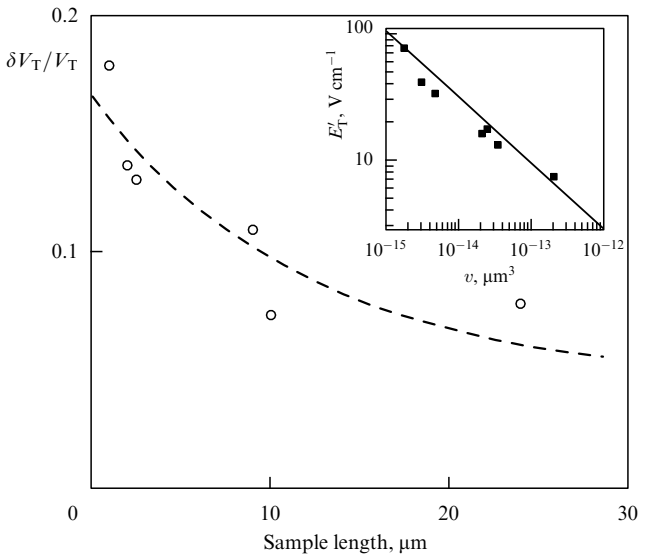

Figure 13. Dependence of the root-mean-square fluctuations of the threshold voltage, $\delta V_T/\langle V_T\rangle$, on the sample length. The inset shows the dependence of the threshold field on the volume of the sample; the solid straight line represents the $E_T \propto v^{-1/2}$ dependence corresponding to equation (19). (Data taken from Ref. [66].)

dimensional pinning, the charge-density wave can be considered rigid. Then its threshold field is determined by the maximum possible force of interaction with impurities:

$$eE_T v n_e = \max_{\phi}\left[\sum_{j=1}^{N} w_i q\cos(qr_j+\phi)\right] \equiv qw_i\left|\left[\sum_{j=1}^{N}\exp(iqr_j)\right]\right|, \quad (18)$$

where n_e is the electron concentration in the CDW, v is the sample's volume, N is the number of impurities within the sample's volume, and the r_j specify the positions of the impurities. Equation (18) shows that the threshold field E_T depends on q. If we take the root-mean-square value of the sum in equation (18), we get

$$\langle E_T^2\rangle^{1/2} = \frac{w_i q}{e v n_e} N^{1/2} = \frac{w_i q}{e}\left(\frac{n_i}{n_e}\right)^{1/2}\left(\frac{1}{n_e v}\right)^{1/2}. \quad (19)$$

We see that the threshold field for samples with a zero-dimensional CDW depends on the volume of the samples rather than on their transverse dimensions. The inset in Fig. 13 shows the dependence $E_T(v)$ for the investigated samples. We see that this dependence is indeed described by equation (19) fairly well. The data make it possible to estimate the pinning energy w_i, which at $n_e = 2\times10^{21}$ cm^{-3} and $n_i/n_e = 10^{-4}$ proves to be equal to $w_i = 3\times10^3$ K.

Replacing E_T with V_T/l and l with Rs/ρ, where R and ρ are, respectively, the resistance of the sample and the resistivity of TaS_3 at room temperature, for the case of zero-dimensional pinning we obtain the relation between the threshold voltage and the sample's resistance at room temperature,

$$\langle V_T^2\rangle^{1/2} = \frac{w_i q}{e n_e}\left(\frac{n_i R}{\rho}\right)^{1/2}, \quad (20)$$

with $\langle V_T\rangle = \sqrt{\pi/2}\langle V_T^2\rangle^{1/2}$. Equation (20) is also true for small TaS_3 samples [66]. Thus, the results of the experiments correspond to the zero-dimensional weak pinning setting in such samples.

The relative value of the fluctuations depends on how close the system is to the case of a zero-dimensional CDW with pinning described by a simple sinusoidal dependence. In the latter case, to which equation (18) corresponds, the standard deviation $\delta V_T \equiv [\langle(V_T - \langle V_T\rangle)^2\rangle]^{1/2}$ is on the order of V_T proper, namely it amounts to $(4/\pi - 1)^{1/2}\langle V_T\rangle \approx 0.52\langle V_T\rangle$ and does not depend on the number of impurities. Since the fluctuations are proportional to the mean, the shape of $V_T(T)$ depends not on the number of impurities but on their positions and the sample dimensions (by analogy with resistance fluctuations in mesoscopic systems).

Note that the value $\delta V_T/\langle V_T\rangle = 0.15 \pm 0.05$ at $l \to 0$ (see Fig. 13) is much smaller than 0.52, the value expected in the case of a sinusoidal potential. In Ref. [66] it was concluded that the results of the experiments do not correspond to the pinning of a rigid CDW to impurities with a sinusoidal pinning potential and that one must allow for local pinning [23], which results in a deviation of the pinning potential from a simple sinusoidal one (see Fig. 2). Such a potential may emerge, for instance, when $\alpha \gg 1$ [see equation (7)] because strong-pinning barriers are surmounted or due to CDW phase slip or thermal fluctuations, which destroys metastability inherent in local pinning (see Fig. 2). In any case, when local metastable states are destroyed, strong pinning contributes nothing, and the pinning force is described by the simple relationship $F_j \propto \phi$. Actually, such a model corresponds to Abe's model [23], which provides a satisfactory description of the results of many experiments [24]. Numerical estimates with such a linear dependence for $F_j(\phi)$ yield $\delta V_T/\langle V_T\rangle = 0.26$, and if we take into account the limited statistics, the spread of the simulation results proves to be in the 0.2–0.3 range, which agrees well with the results of the experiments [66].

3.11 Absolute negative resistance

Studies of CDW dynamics over distances of about 1 μm or less have led to the discovery of absolute negative resistance [18]. In these experiments, the nonlinear conduction of short segments of TaS_3 and $NbSe_3$ samples was explored. In the studies of long segments (more than 10 μm long), the ordinary current–voltage characteristics were recorded. However, when reducing the distance between the potential contacts to several micrometers, the shape of the current–voltage characteristics varied dramatically from segment to segment, and for some segments, sections of absolute negative resistance were recorded. As an example, Fig. 14 shows the current–voltage characteristics of two adjacent segments of a TaS_3 crystal, which exhibits such behavior. Clearly, at $I > 3$ μA (Fig. 14a) the voltage across one of the segments becomes negative. As a rule, the voltage across the adjacent segment exceeds the mean value, which is depicted by the dashed curve. Of course, such behavior is observed only when the measurements are carried out in a four-contact configuration.

The qualitative explanation for negative conductivity is as follows [18]. It appears because the motion of the CDW and the motion of the quasiparticles depend on different potentials. At low temperatures the CDW motion is determined by the difference in the electrostatic potentials Φ, while the motion of the quasiparticles depends on the distribution of

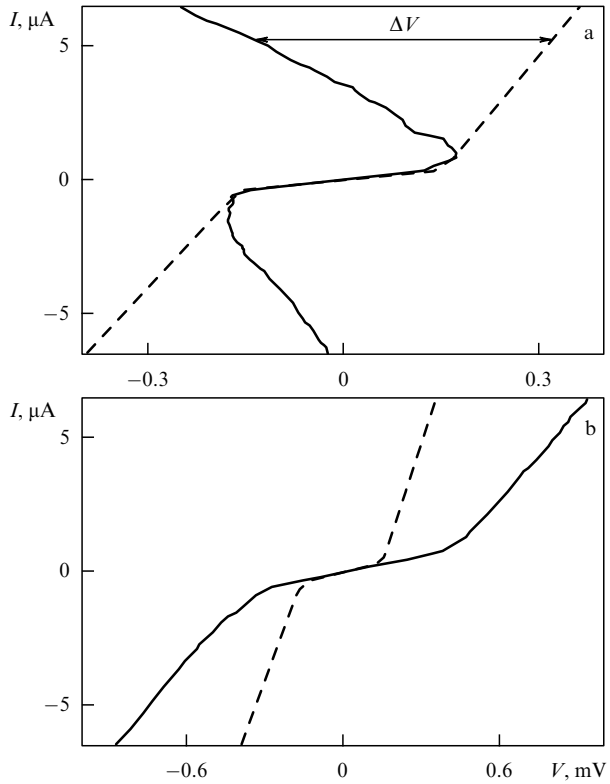

Figure 14. Current – voltage characteristics of two 1-μm long adjacent segments of the TaS_3 crystal with a cross-sectional area of 0.5 μm^2 at $T = 120$ K. The dashed curve shows the 'mean' current – voltage characteristic obtained by multiplying the voltage measured across the length of 36.1 μm by 1/36.1. (Data taken from Ref. [18].)

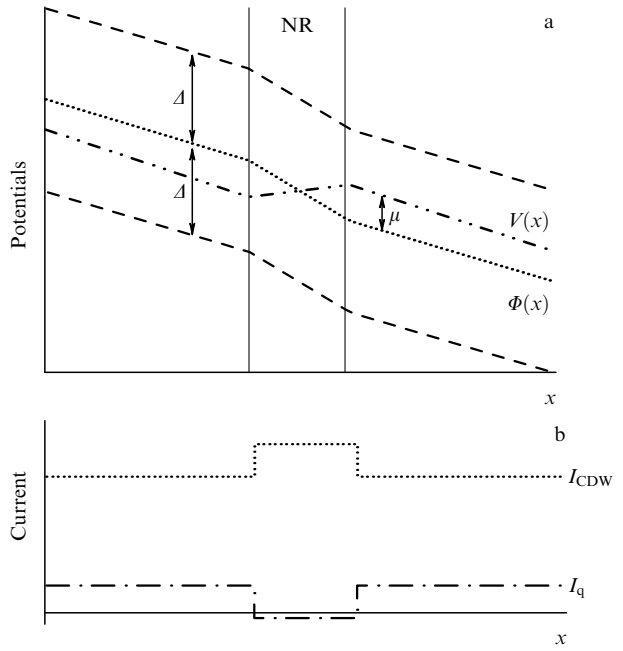

Figure 15. Distributions of potentials (a) and currents (b) along a sample with a section of negative resistance (NR).

the electrochemical potential $V(x)$ measured with voltmeters. The following conclusions about the distribution of potentials and currents along the sample can be drawn on the basis of the results of measurements (Fig. 15). First, the slope dV/dx in the negative-resistance region has a sign opposite to that in the other part of the sample. This implies that the quasiparticle current I_q in this region also flows in the opposite direction. Since the total current I must remain constant, the current I_{CDW} transported by the CDW is higher in the negative-resistance region than in the other part of the sample.

Van der Zant et al. [18] argued that the assumption that the proportionality factor K linking the CDW current and the CDW phase velocity, $I_{CDW} = K\dot{\phi}$, is constant along the sample leads to a contradiction between the sign of the CDW deformation and the nature of the CDW phase slip: at $K(x) = \text{const}$, Fig. 15 clearly shows that stretching the CDW would lead to the disappearance of CDW periods while compressing the CDW would lead to the creation of new periods; in reality, the opposite situation should be observed. This implies that the origin of the effect lies in the existence of the coordinate dependence of the factor K. Such a dependence can be caused, for instance, by macroscopic defects or by substantial changes in the impurity concentration in the negative-resistance region. If we assume that in the negative-resistance region this factor is somewhat larger, $I_{CDW} = (1 + a)K\dot{\phi}$, then for the difference in the electrochemical potential in the negative-resistance region we obtain

$$V = R_0(I_q - aI_{CDW}),$$

where R_0 is the linear resistance of the negative-resistance section. The above equation shows that with a sufficiently high CDW current the drop in voltage across the segment of interest may change its sign.

The results of experiments confirm the value $a \approx 0.1$, while the theories [96, 97] that take into account the contribution of the quasiparticles to K yield values that are several orders of magnitude smaller. The reasons for such a discrepancy are yet to be clarified. A similar discrepancy between the predictions of the theory and the experimental data exists in the explanation of the contribution of CDW sliding to the Hall effect [98, 99] caused by the contribution of quasiparticles to the current carried by the CDW [96, 97].

3.12 Structures of the field-effect transistor type

Experimental studies of the electrophysical properties of quasi-one-dimensional conductors with CDWs can be extended substantially by fabricating artificial structures based on such conductors. One of the most promising areas of research in this field is the formation of structures in which the CDW parameters can be controlled by external influence, such as an electric field, for instance. In this section we discuss the properties of field-effect transistors based on the quasi-one-dimensional conductors $NbSe_3$ and TaS_3 [67]. It was found that such structures exhibit unusual enhancement of the field effect by several orders of magnitude when the channel transforms from the metallic state to the Peierls state, with the response gain appearing in the collective conduction, while single-particle conduction remains practically unchanged.

Figure 16 shows the current – voltage characteristics of a channel fabricated from a thin $NbSe_3$ sample at a temperature $T = 30$ K for different gate voltages V_G. As the gate voltage changes, the corresponding variation of linear conduction related to the single-particle current is too small to be noticed on the scale of Fig. 16. At the same time, the CDW collective response strongly depends on V_G. When the voltage across

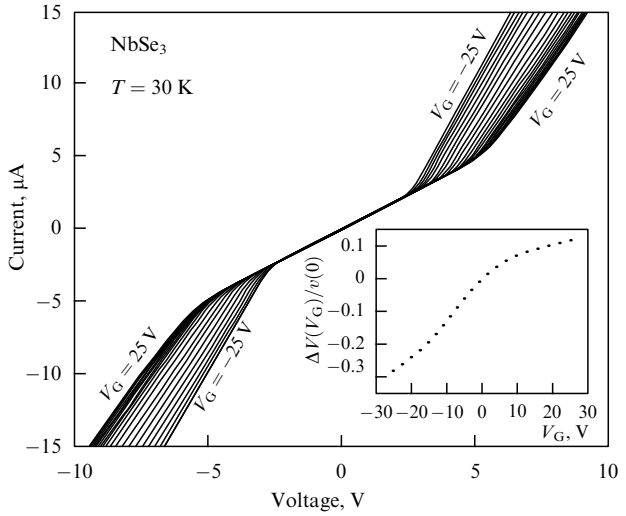

Figure 16. Current–voltage characteristics of the $NbSe_3$ crystal with a cross-sectional area of 1.1×10^{-3} μm^2 at $T = 30$ K for gate voltages V_G varying from −25 to 25 V with an increment of 2.5 V. The gate voltage causes substantial modulation of the CDW sliding threshold field E_T but has almost no effect on the linear conductivity at voltages below the threshold value. The inset shows the dependence of $[V(V_G, I_c) - V(0, I_c)]/V(0, I_c)$ on the gate voltage at $I_c = 6$ μA, which is used to estimate $[E_T(V_G) - E_T(0)]/E_T(0)$.

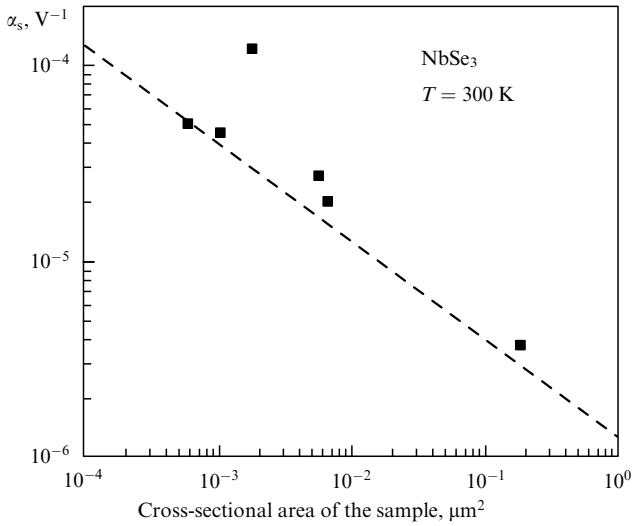

Figure 17. Dependence of the relative sensitivity α_s of single-particle (linear) resistance to the gate voltage, V_G, on the cross-sectional area of the sample. The dashed curve represents the prediction made by equation (21) with $d = \sqrt{s}$. $T = 300$ K.

the channel is close to the threshold value at which CDW sliding begins, this sliding can be switched on or off by changing V_G. Since the nonlinear sections in the current–voltage characteristics at different values of V_G are practically parallel to each other, the predominant result of the changes in V_G is the modulation of the threshold voltage V_T.

The inset in Fig. 16 shows a typical dependence of the voltage variation needed for transporting the current I_c,

$$\frac{V(V_G, I_c) - V(0, I_c)}{V(0, I_c)} \approx \frac{E_T(V_G) - E_T(0)}{E_T(0)}$$

on the gate voltage V_G with the nonlinear current being $I_c = 6$ μA. The quantity monotonically depends on V_G at $|V_G| < 20$ V and is positive at $V_G > 0$.

Following Ref. [67], we analyze the field effect at room temperature, at which $NbSe_3$ is in the metallic state. The gate voltage V_G charges the channel to a level that is sufficiently high to be able to screen the transverse electric field. The charge induced by V_G changes the resistance of the channel, with the relative sensitivity of the linear resistance to V_G being

$$\alpha_s \equiv \frac{1}{R}\,\frac{\partial R}{\partial V_G} \approx \frac{\epsilon\epsilon_0}{e n_e d\, d_\epsilon}\,, \qquad (21)$$

where ϵ_0 is the permittivity of the vacuum, ϵ and d_ϵ are, respectively, the dielectric constant and the thickness of the insulator layer, and d is the sample thickness.

Figure 17 shows the sensitivity α_s, measured at room temperature, as a function of the cross-sectional area s of the $NbSe_3$ channel. The dashed curve represents the prediction made by equation (21) at $\epsilon = 3.85$ and $d = \sqrt{s}$. Clearly, this curve agrees with the values of sensitivity obtained through experiments. Substituting $d = \sqrt{s}$ into equation (21) yields a smaller value of α_s, since the thickness of a $NbSe_3$ crystal is usually much smaller than the crystal's width. The sign of the effect points to the hole nature of conduction and agrees with the sign of the Hall effect [100]. The observed quantitative agreement makes it possible to conclude that surface states play a minor role in screening the transverse electric field. For a gate voltage of 15 V and a channel cross-sectional area of 10^{-3} μm^2, the induced charge amounts to approximately 0.1% of the total charge of the current carriers. This charge screens the transverse electric field on the Thomas–Fermi length, which in $NbSe_3$ is about 1 nm.

Similar behavior in conduction has been observed in TaS_3. As in $NbSe_3$, both linear (single-particle) and nonlinear conductivities change as the gate voltage varies. The sensitivity of the linear and nonlinear conductivity is comparable to the values observed in $NbSe_3$. In the metallic state at $T > T_P$, the sign of the sensitivity of the linear conductivity to the gate voltage corresponds to hole conduction and coincides with the sign of the Hall effect [94].

At temperatures $T < T_P$, the transverse electric field is screened both by single-particle excitations and by the CDW. The field effect was first considered theoretically by Brazovskii and Matveenko [101] before the measurements described above [67]. It was found that CDWs participate in the screening of transverse fields. This conclusion is corroborated by the results of experiments. Indeed, the total screening charge depends only on V_G and not on the temperature. The density of single-particle excitations in $NbSe_3$ at temperatures between T_{P2} and 20 K decreases by a factor greater than 1000. But, as the results given in Ref. [67] imply, the temperature dependence of the linear-conduction sensitivity to the gate voltage is much weaker. Thus, at low temperatures almost all screening is done by the CDW.

Figure 17 shows that the single-particle density of states changes to the same measure as linear conductivity. If there were a similar correspondence between the CDW conductivity and the charge density in the CDW, the collective-conduction sensitivity at temperatures below the Peierls transition point would be comparable to the linear-conduction sensitivity in the metallic state at $T > T_{P1} = 145$ K. However, experiments have shown (see Fig. 16) that the collective-conduction sensitivity exceeds the single-particle-conduction sensitivity in the metallic state by more than

three orders of magnitude. This constitutes the most important feature of the field effect in quasi-one-dimensional conductors. Therefore, the question arises of how such relatively small variations in the CDW charge density (on the order of 0.1%) generate such large variations (up to 100%) in the CDW conductivity. Adelman et al. [67] considered several possible explanations.

1. To screen the transverse field, the charge density in the CDW must change in the transverse direction. Since the charge density in a CDW is proportional to the CDW wave vector, transverse changes in the wave vector lead to the appearance of CDW dislocations [101]. The emergence of dislocations may change the CDW conductivity by causing additional pinning or, to the contrary, by facilitating depinning (e.g., near the surface or near contacts or structural defects). In any case, the variation in the CDW conductivity must be proportional to the dislocation density and must be an even effect with respect to V_G. However, as Fig. 16 shows, an odd effect is observed.

2. The variations in the CDW charge caused by the transverse field may change the CDW pinning due to the fact that the CDW moves closer to commensurability with the crystal lattice. For a CDW that is formed in $NbSe_3$ at $T < T_{P2}$, the wave vector $q = 0.259$ exceeds the value $q = 0.250$ corresponding to such commensurability by approximately 3%. Changing the wave vector by 3% requires changing the concentration n_e by 3%. Such variation is substantially larger than the above estimates of the maximum variations of the current carrier concentration (0.1%). Furthermore, since E_T is higher at positive gate voltages V_G, according to this mechanism a low-temperature CDW in $NbSe_3$ is formed only on the hole side of the Fermi surface and not on the electron side, as opposed to the case observed in experiments (see Ref. [1]).

3. The variation in the charge density in the CDW near the crystal's surface caused by a transverse field may change the charge modulation amplitude near the surface and hence change the degree of surface CDW pinning near the surface facing the gate. Nevertheless, there is no convincing proof that surface pinning actively participates in the formation of the threshold field E_T in $NbSe_3$.

4. Such a large observed variation of CDW conductivity is caused by the variations in bulk pinning due to the variations in the CDW order parameter Δ. The threshold field E_T in the case of weak pinning can be written as follows [102, 103]:

$$E_T \propto \frac{\Delta^{4/(4-D)}}{K^{4/(4-D)-1}} \tag{22}$$

[see equation (2)]. The relative threshold-field sensitivity to V_G can then be approximately written as follows:

$$\frac{1}{E_T}\,\frac{dE_T}{dV_G} \approx \left[\left(\frac{4}{4-D}\right)\frac{1}{\Delta} - \left(\frac{4}{4-D}-1\right)\frac{1}{K}\,\frac{dK}{d\Delta}\right]\frac{d\Delta}{dV_G}\,. \tag{23}$$

Since $dK/d\Delta \approx 0$ for $NbSe_3$ [54, 104], the threshold-field sensitivity must have the same sign as $d\Delta/dV_G$. The results of measurements reported in Ref. [67] show that $d\Delta/dV_G$ is positive, which agrees with the condition $(1/E_T)\,dE_T/dV_G > 0$.

According to estimates, the amplitude of order-parameter variations when voltage is applied to the gate by such a mechanism may be substantial: for $V_G = 15$ V the data in Fig. 16 assume [3] a 10% change in Δ. Although experimental verification of this estimate is difficult, we note that in experiments involving the quasi-one-dimensional conductor $K_{0.3}MoO_3$ the volume variations caused by hydrostatic pressure, which create comparable variations in the charge density, also lead to comparable variations in the order parameter [105]. However, applying pressure changes not only the current carrier concentration. Hence, a detailed quantitative comparison of these results with the results of field-effect studies is difficult.

For the gate voltage to have an effect on the CDW in the way described above, the transverse electric field must penetrate the $NbSe_3$ channel to large depths. The penetration depth d_p depends on the balance between the electric field energy U_E and the dislocation energy U_d [67]. The electric field energy is proportional to V_G squared and, hence, $U_E \propto d_p V_G^2$. The total induced charge, which is proportional to V_G, can be screened either by a large number of dislocations near the channel's surface or by a small number of dislocations inside the sample, since the charge related to an edge dislocation is proportional to the depth d_p of the dislocation's penetration into the channel. Hence, $d_p N_d \propto V_G$. And since the dislocation energy is proportional to the total number of dislocations N_d, we have $U_d \propto N_d \propto V_G/d_p$. Minimization of the total energy yields $d_p \propto V_G^{-1/2}$. Thus, under small gate voltages the contribution U_d is predominant and, hence, both the dislocations and the electric field penetrate the channel to great depths. When the gate voltage is large, the contribution U_E across the gate is predominant, and the dislocations concentrate near the channel's surface. This behavior corresponds to a nonlinearity that is present in the dependence of the threshold field on the gate voltage, shown in the inset in Fig. 16.

3.13 Aharonov – Bohm effect in CDW sliding through a system of columnar defects

The question of how quantum effects contribute to the physical properties of quasi-one-dimensional conductors with CDWs is one of the most interesting questions in this area of solid state physics. Many of the observed properties of CDWs can be explained without bringing in quantum mechanics. The Aharonov – Bohm effect in quasi-one-dimensional conductors has been examined by Bogachek et al. [106] for the case of ring structures. It was found that there is quantization of flux in such a ring with a period of $2e$. An attempt to observe this effect (true, in a sample with a different configuration) was made by Latyshev et al. [79]. They studied linear and nonlinear conduction of an $NbSe_3$ crystal with lattice defects created by irradiating the crystals with 250-MeV xenon ions. Such irradiation leads to the appearance of columnar defects, which are cylindrical regions of amorphized $NbSe_3$ 16 ± 2 -nm in diameter. It turned out that the conductivity of the irradiated samples as a function of the magnetic field contained a periodic component with a period of 8.6 T. Figure 18 shows an example of such a dependence. Oscillations were observed only in the nonlinear conduction regime and reached their maximum value at currents exceeding the threshold current by a factor of two to three. With much higher currents (the curve for 900 μA) no oscillations were observed.

[3] In accordance with the results of studies of the finite-size effect in $NbSe_3$, it is assumed in equation (23) that $D = 2$.

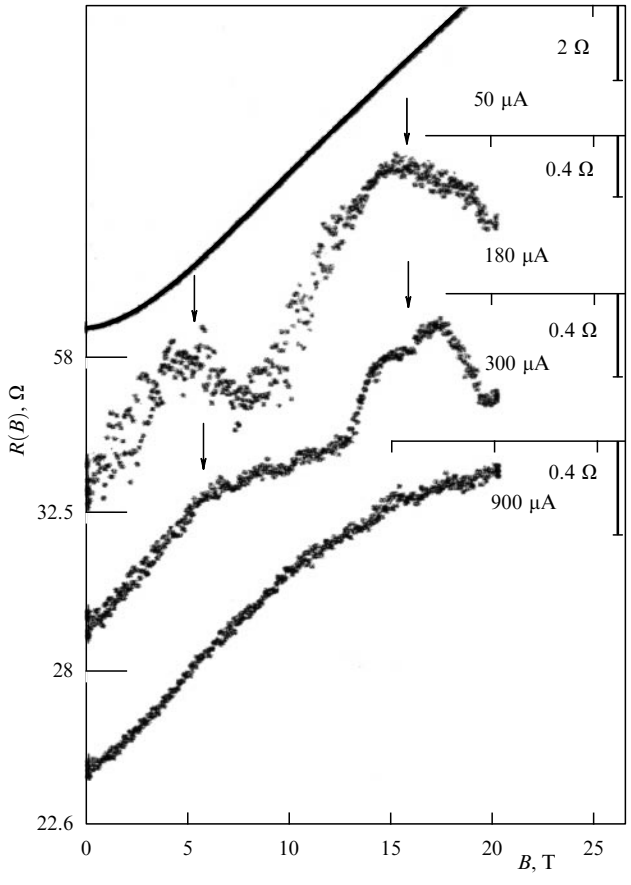

Figure 18. Dependence of resistance on the magnetic field in the linear conduction region ($I = 50$ μA) and in the nonlinear conduction region (180, 300, and 900 μA) a $NbSe_3$ crystal with columnar defects at $T = 52$ K. (Data taken from Ref. [79].)

The oscillation period corresponds to the effective carrier charge of $2e$, which coincides with the estimates in the theoretical work of Bogachek et al. [106], in which quantization of magnetic flux in a ring of a quasi-one-dimensional conductor was considered. Latyshev et al. [79] concluded that the observed oscillations attest to the quantum nature of CDW motion. The disappearance of the effect at high values of CDW current was attributed to the loss of coherence in a high electric field. So far we have no theory to describe the quantum oscillations of CDW conductivity in the geometry used in the experiments by Latyshev et al. [79].

Note that the observation of negative resistance in quasi-one-dimensional conductors [18] makes possible a new approach to interpreting the results of studies of nonlinear-conduction oscillations [79]. The results of the work of van der Zant et al. [18] imply that in quasi-one-dimensional conductors there is a strong relationship between CDW currents and the currents of normal carriers. For this reason, we can expect that by changing the conditions in which the current of normal carriers flows we can influence the nonlinear current. In a metal such as aluminum, the typical value of the dephasing length of the electron wave function, L_ϕ, is about 1 μm [107] at $T = 5$ K, and as the temperature rises this length decreases by a power law to 0.2 μm at 20 K (see also Ref. [108]). Extrapolating this dependence to $T = 50$ K, we get $L_\phi \sim 100$ nm. Assuming that in $NbSe_3$ the value of L_ϕ is of the same order of magnitude, we conclude that persistent currents can flow around columnar defects. These currents oscillate with the period corresponding to the charge e. The CDW motion in the region with macroscopic defects is closely related to the motion of quasiparticles, which are responsible for energy dissipation. In the approximation linear in the persistent current, the current oscillations have no effect on the CDW motion. However, in the second-order approximation, we can expect an oscillating contribution of the current to the CDW motion, with the respective oscillation period being smaller by a factor of two, i.e., corresponding to the charge $2e$, which agrees with the results of observations by Latyshev et al. [79]. Note that the nonlinearity in CDW — persistent current coupling is related to large CDW deformations in the region with columnar defects. Such a scenario provides an explanation of the effect without the concept of CDW motion across atomic chains, required for the effect to be explained as the consequence of quantum CDW motion. Unfortunately, as in the case of negative resistance, the absence of a quantitative theory makes it impossible to estimate the oscillation amplitude.

3.14 Finite-size effect in the CDW phase slip

The dependence of the phase slip voltage on the distance between the current contacts $V_{ps}(l)$ has been studied by Mantel et al. [78] in $NbSe_3$ samples with distances between the current contacts as small as 0.5 μm. The results are shown in Fig. 19. It turned out that the phase slip voltage strongly depends on the distance between the contacts and decreases fourfold as the contacts move closer to a separation $l = 0.5$ μm.

Such behavior in the voltage V_{ps} does not fit the phase slip theory of Ramakrishna et al. [52], according to which V_{ps} should grow as the distance between the current contacts decreases because of the narrowing of the region of maximum CDW deformation, where phase slip takes place.

A decrease in the measured value of the phase slip voltage may occur because of the spatial inhomogeneity in the current flow in the shortest samples studied by Mantel et al. [78], whose width exceeds the length in the isotropic representation by a factor greater than four. However, according to the

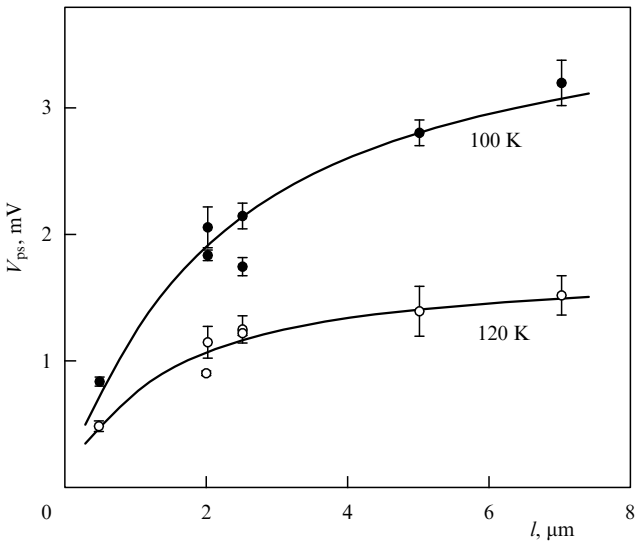

Figure 19. Dependencies of the phase slip voltage on the distance between the current contacts in $NbSe_3$. (Data taken from Ref. [78].)

estimates [78], the contribution of the geometrical factor does not exceed 0.1 mV. The authors concluded that the most probable cause of the finite-size effect is the correlations between the acts of phase slip on the current contacts that are separated by distances smaller than the phase correlation length.

Artemenko [109] recently suggested an explanation for the effect. The microscopic theory of current conversion was used, and correlations that exist between processes of CDW phase slip on contacts separated by small distances were taken into account. It was found that in this case the voltage V_{ps} in short samples nonmonotonically depends on the CDW current and at large values of the current proves to be strongly dependent on the distance between the current contacts for $l \lesssim 1$ μm, with V_{ps} decreasing with this distance.

In addition to the analysis of the results given in Refs [78, 109], we note that an effect equivalent to the appearance of an additional voltage δV as the sample gets shorter may also emerge as a result of a finite-size effect under weak pinning. Indeed, in the case of zero-dimensional pinning and ignoring V_{ps}, from equation (19) we obtain $V_T \propto \sqrt{l}$. Writing the contribution of pinning for $l < L_\parallel$ in the form $V_T = E_T l + \delta V$, we find that $\delta V = E_T[(lL_\parallel)^{1/2} - l]$. For instance, for the sample examined in Ref. [78], $E_T = 1.2$ V cm^{-1}, and the value of V_{ps} measured at $l = 2$ μm amounts to 0.9 mV. Here the expected value of the length-dependent addition at $L_\parallel = 10$ μm amounts to $\delta V = 0.25 E_T L_\parallel \approx 0.3$ mV, which is 50% of the real value of V_{ps}. In the case of one-dimensional pinning (the length and one of the transverse dimensions of the sample are smaller than the respective phase correlation lengths), $\delta V E_T[(L_\parallel^2 l)^{1/3} - l]$, and hence, for the sample parameters given in Ref. [78] we get $\delta V = 0.45$ mV, which is 100% of V_{ps}.

Thus, the weak pinning contribution, to depends on the sample length, proves to be comparable to $V_{ps}(l)$, so that this contribution should be taken into account in a quantitative analysis of the results of measurements of $V_{ps}(l)$ [78]. Here, if we remain within the above simple approach to the estimate of the contribution of weak pinning [4], δV is positive, i.e., the actual value of $V_{ps}(l)$ proves to be smaller than the measured value, and the finite-size effect in the dependence of the CDW phase slip voltage on the distance between the current contacts is retained.

3.15 Crossover to one-dimensional conduction in thin samples

A special area of research in the physics of quasi-one-dimensional conductors is the physical properties of samples with extremely small transverse dimensions, samples that consist, in the limiting case, of a single conducting filament. The interest in such objects stems from the unusual properties that are predicted for one-dimensional electron systems: the disappearance of single-particle excitations (quasiparticles) with collective conduction retained, the appearance of spin – charge separation, and other properties [110]. Quasi-one-dimensional conductors are convenient objects for such studies, since reduced-dimensionality effects are initially inherent in them.

The dramatic change of the properties of $NbSe_3$ and TaS_3 caused by a reduction in the transverse dimensions of the samples was first demonstrated in Ref. [76]. It turned out that, as the transverse dimensions of $NbSe_3$ samples are reduced to values corresponding to the value of the resistance per unit length, R/l, on the order og 10^3 Ω μm^{-1}, the temperature dependence of the resistance and the shape of the current – voltage characteristic undergo dramatic changes. Instead of the 'metallic' behavior of the dependence $R(T)$, characteristic of bulk $NbSe_3$ samples, with two maxima corresponding to two phase transitions, apparent dielectrization of the energy spectrum occurs, with the temperature and voltage dependencies of the resistance of such thin samples described by laws that closely resemble power laws, $R(T) \propto T^{-\alpha}$ and $R(E) \propto E^{-\beta}$, where R varies by three or four orders of magnitude (Fig. 20). It is this behavior that is expected of one-dimensional metallic systems with impurities [110]. Note that in the one-dimensional case the impurities are interpreted as tunneling barriers, so that the shape of the current – voltage characteristics and the temperature dependence of the resistance are determined by specifically one-dimensional power dependencies of the tunnel density of states on the energy. The measurements described in Ref. [76] were carried out with $NbSe_3$ samples, which were fabricated by splitting and additional thinning via plasmochemical etching.

The dependence of the resistance of $NbSe_3$ samples on the sample width was studied in Ref. [77]. The width variation was provided by a focused ion beam. The results of the first observations (see Ref. [76]) were reproduced, and the crossover to one-dimensional behavior was observed even in relatively large samples whose width was on the order of 100 nm. In addition, it was found that such power laws can also be observed in bulk $NbSe_3$ samples after they are cut in the transverse direction by a focused ion beam and connected by their ends with platinum. After this procedure is completed, the properties of the sample change over a distance on the order of 10 μm in the direction of the highest conduction

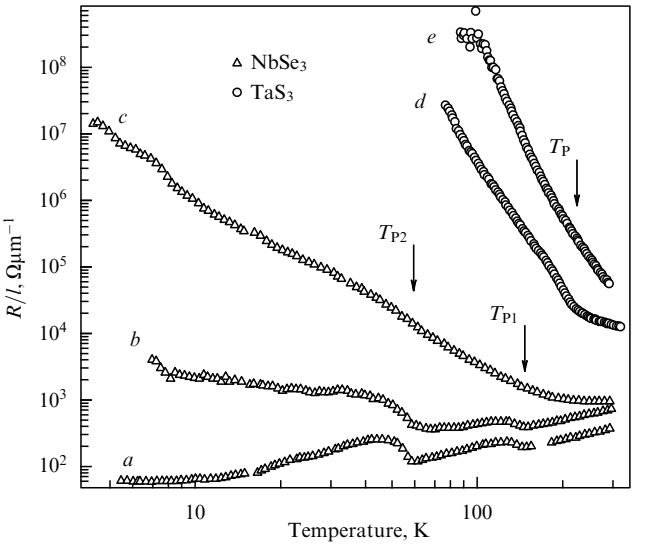

Figure 20. Temperature dependencies of the resistance of thin samples of the quasi-one-dimensional conductors $NbSe_3$ and TaS_3. The arrows indicate the positions of the Peierls transition points for bulk samples. The curves *a*, *b*, and *c* correspond to three consecutive stages of thinning of the $NbSe_3$ sample in SF_6 plasma. (Data taken from Ref. [76].)

[4] These estimates are based on the relations for D-dimensional pinning in samples with $l \leqslant L_\parallel$ ($D = 0$, 1) and $(D+1)$-dimensional pinning for $l \geqslant L_\parallel$. Such an approach leads to a nonphysical dependence with a break in the derivative at $l = L_\parallel$.

away from the cut. The temperature and field dependencies of the conductivity of such a modified region are described by the same laws as the conductivity of one-dimensional electron systems, and they even obey scaling relations [111].

The effect of impurities on the conductivity and the spatial distribution of impurities in $NbSe_3$ were studied by Gong et al. [112]. Investigation of the surface of doped $NbSe_3$ with an atomic-force microscope revealed the ordering of impurities dependent on their concentration, with the period of the observed structure sometimes amounting to several lattice periods. Turgut and Falicov [113] did a theoretical study of the effects of interaction between the impurities in a quasi-one-dimensional metal, effects that come into play because of the specific polarizability of the one-dimensional electron gas, which leads to slowly decaying Friedel oscillations. It was found that, depending on the concentration and valence of the impurities in a quasi-one-dimensional metal, order in the positions of the impurities may arise.

Further studies (see Ref. [74]) showed that the conductivity of even thinner $NbSe_3$ and TaS_3 samples fabricated via splitting in an electric field ($R/l \sim 2 \times 10^5\ \Omega\ \mu m^{-1}$, which corresponds to $s \sim 10\,nm^2$) cannot be described by power laws, but is quite satisfactorily described by Mott's law for variable range hopping conduction in the one-dimensional case, $R \propto \exp(-[T_0/T]^{1/(1+D)})$, $D \approx 1$. Note that it is namely such behavior of conductivity that is expected for one-dimensional metals with high impurity concentration [114]. The question whether the model introduced in Ref. [114] can be used to describe the samples employed in the study of Ref. [74] remains open. We also note that in bulk crystals of quasi-one-dimensional conductors with CDWs, hopping conduction was observed earlier in the linear conductivity of $Fe_{0.25}Nb_{0.75}Se_3$ [115] ($T < 140$ K) and orthorombic TaS_3 with a high impurity concentration (the threshold field $\sim 10\ V\ cm^{-1}$) at $T < 20$ K [116].

Thus, quasi-one-dimensional conductors of extremely small dimensions exhibit properties predicted for one-dimensional electron systems. These properties may arise because of finite-size effects leading to a rise in fluctuations, which inhibit the formation of a three-dimensionally ordered CDW. The injection of impurities into a quasi-one-dimensional metal may cause dielectrization of the electron spectrum and may also lead to effects characteristic of one-dimensional systems. Such behavior reflects the specific nature of quasi-one-dimensional conductors and requires further investigation.

4. Conclusion

The study of finite-size effects in quasi-one-dimensional conductors with CDWs has proved to be an exceptionally fruitful area of research and has encompassed a considerable part of the physics of quasi-one-dimensional conductors. At the same time, there remain problems whose solution can substantially enrich our understanding of the physics of quasi-one-dimensional conductors. For instance, within the scope of existing ideas about the kinetics of charge-density waves it so far seems impossible to quantitatively describe negative resistance, collective response in the field effect, and oscillations of collective conductivity in a magnetic field. Moreover, we still have to examine finite-size effects in CDW creep; there is still no theory of CDW phase slip, which could be used to describe the experimentally observed dependencies of the nonlinear current on the phase slip voltage V_{ps} and the dependence of V_{ps} on the distance between the current contacts; we still do not know what role phase slip plays in the finite-size effects involving the Peierls transition; and, finally, only the first results pertaining to the physical properties of extremely small, thin quasi-one-dimensional conductors have been obtained.

The author is grateful to S N Artemenko and V Ya Pokrovskiĭ for the time they spent in reading the manuscript and for the useful remarks and discussions. This work was made possible by the financial support of the Russian Fund for Basic Research (Grants 01-02-17771, 0.4-0.2-16509), NWO, and INTAS.

References

1. Monceau P (Ed.) *Electronic Properties of Inorganic Quasi-One-Dimensional Compounds* Pt. II (Dordrecht: D. Reidel, 1985) p. 139; Grüner G *Rev. Mod. Phys.* **60** 1129 (1988); **66** 1 (1994)
2. Brazovskii S, Kirova N, Monceau P (Eds) *Proc. of the 3rd Intern. Workshop on Electronic Crystals*: *ECRYS-2002, St. Flour, France, Sept. 2–7, 2002* (J. Phys. IV (France), Vol. 12, Pr9) (Les Ulis: EDP Science, 2002); Brazovski S, Monceau P (Eds) *Proc. of the 2nd Intern. Workshop on Electronic Crystals*: *ECRYS'99, La Colle-sur-Loup, France, May 31–June 5, 1999* (J. Phys. IV (France), Vol. 9, Pr10) (Les Ulis: EDP Science, 1999); Brazovskii S, Monceau P (Eds) *Proc. of the 1st Intern. Workshop on Electronic Crystals*: *ECRYS'93* (J. Phys. IV (France), Vol. 3, Coll. 2) (Les Ulis: EDP Science, 1993)
3. McCarten J et al. *Phys. Rev. B* **46** 4456 (1992)
4. Brill J, in *Handbook of Elastic Properties of Solids, Liquids, and Gases* (Editors-in-Chief M Levy, H E Bass, R R Stern) Vol. II *Elastic Properties of Solids*: *Theory, Elements and Compounds, Novel Materials, Alloys, and Building Materials* (Ed. M Levy) (San Diego: Academic Press, 2001) Ch. 10, p. 143
5. Latyshev Yu I, Sinchenko A A *Pis'ma Zh. Eksp. Teor. Fiz.* **75** 714 (2002) [*JETP Lett.* **75** 593 (2002)]
6. Peierls R E *Quantum Theory of Solids* (Oxford: Clarendon Press, 1955) [Translated into Russian (Moscow: IL, 1956)]
7. Sato M et al. *J. Phys. C*: *Solid State Phys.* **18** 2603 (1985)
8. Larkin A I *Zh. Eksp. Teor. Fiz.* **58** 1466 (1970) [*Sov. Phys. JETP* **31** 784 (1970)]
9. Efetov K B, Larkin A I *Zh. Eksp. Teor. Fiz.* **72** 2350 (1977) [*Sov. Phys. JETP* **45** 1236 (1977)]
10. Fukuyama H, Lee P A *Phys. Rev. B* **17** 535 (1978)
11. Lee P A, Rice T M *Phys. Rev. B* **19** 3970 (1979)
12. Wang Z Z et al. *J. Phys. Lett.* (Paris) **44** L311 (1983)
13. Higgs A W, Gill J C *Solid State Commun.* **47** 737 (1983)
14. Ong N P *Phys. Rev. B* **18** 5272 (1978)
15. Artemenko S N, Volkov A F *Zh. Eksp. Teor. Fiz.* **80** 2018 (1981) [*Sov. Phys. JETP* **53** 1050 (1981)]
16. Sneddon L *Phys. Rev. B* **29** 719 (1984)
17. Zhang X J, Ong N P *Phys. Rev. Lett.* **55** 2919 (1985); Fleming R M et al. *Phys. Rev. B* **33** 5450 (1986)
18. van der Zant H S J et al. *Phys. Rev. Lett.* **87** 126401 (2001)
19. Artemenko S N, Pokrovskii B Ya, Zaitsev-Zotov S V *Zh. Eksp. Teor. Fiz.* **110** 1069 (1996) [*JETP* **83** 590 (1996)]
20. Artemenko S N, Volkov A F *Pis'ma Zh. Eksp. Teor. Fiz.* **33** 155 (1981) [*JETP Lett.* **33** 147 (1981)]
21. Grüner G, Zawadowski A, Chaikin P M *Phys. Rev. Lett.* **46** 511 (1981)
22. Wu W-Y, Jánossy A, Grüner G *Solid State Commun.* **49** 1013 (1984)
23. Abe S *J. Phys. Soc. Jpn.* **54** 3494 (1985); **55** 1987 (1986)
24. Tucker J R, Lyons W G, Gammie G *Phys. Rev. B* **38** 1148 (1988)
25. Zaitsev-Zotov S V, Remenyi G, Monceau P *Phys. Rev. Lett.* **78** 1098 (1997)
26. Gill J C *Synthetic Met.* **43** 3917 (1991)
27. Larkin A, Brazovskii S *Solid State Commun.* **93** 275 (1995)
28. Sweetland E et al. *Phys. Rev. Lett.* **65** 3165 (1990)
29. Pokrovskii V Ya, Zaitsev-Zotov S V *Synthetic Met.* **29** F439 (1989)
30. Zaitsev-Zotov S V *Phys. Rev. Lett.* **71** 605 (1993)
31. Nattermann T *Phys. Rev. Lett.* **64** 2454 (1990)

32. Gill J C *J. Phys. IV* (France) **12** Pr9-161 (2002)
33. Duan J-M *Phys. Rev. B* **48** 4860 (1993)
34. Maki K *Phys. Lett. A* **202** 313 (1995)
35. Matsukawa H, in *Quantum Coherence and Decoherence: Foundations of Quantum Mechanics in the Light of New Technology. Proc. of the 5th Intern. Symp., ISQM-Tokyo'95, Saitama, Japan, Aug. 21–24, 1995* (Eds K Fujikawa, Y A Ono) (Amsterdam: Elsevier, 1996) p. 115, 121
36. Matsukawa H et al. *J. Phys. IV* (France) **9** Pr10-161 (1999)
37. Zaitsev-Zotov S V, Remenyi G, Monceau P *Phys. Rev. B* **56** 6388 (1997)
38. Lemay S G et al. *Phys. Rev. Lett.* **83** 2793 (1999)
39. Artemenko S N, Volkov A F *Zh. Eksp. Teor. Fiz.* **81** 1872 (1981) [*Sov. Phys. JETP* **54** 992 (1981)]
40. Itkis M E, Nad' F Ya, Pokrovskii V Ya *Zh. Eksp. Teor. Fiz.* **90** 307 (1986) [*Sov. Phys. JETP* **63** 177 (1986)]
41. Borodin S V, Zaitsev-Zotov S V, Nad' F Ya *Zh. Eksp. Teor. Fiz.* **93** 1394 (1987) [*Sov. Phys. JETP* **66** 793 (1987)]
42. Feinberg D, Friedel J *J. Phys.* (Paris) **49** 485 (1988)
43. Horovitz B, Krumhansl J A, Domany F *Phys. Rev. Lett.* **38** 778 (1977)
44. Brazovskii S A, Matveenko S I *Zh. Eksp. Teor. Fiz.* **99** 887 (1991) [*Sov. Phys. JETP* **72** 492 (1991)]
45. Ong N P, Verma G, Maki K *Phys. Rev. Lett.* **52** 663 (1984)
46. Gor'kov L P *Pis'ma Zh. Eksp. Teor. Fiz.* **38** 76 (1983) [*JETP Lett.* **38** 87 (1983)]
47. Artemenko S N, Volkov A F, Kruglov A N *Zh. Eksp. Teor. Fiz.* **91** 1536 (1986) [*Sov. Phys. JETP* **64** 906 (1986)]
48. Maki K *Physica B + C* **143** 59 (1986)
49. Brazovskii S, Matveenko S *J. Phys. I* (France) **2** 409, 725 (1992)
50. Artemenko S N, Gleisberg F *Phys. Rev. Lett.* **75** 497 (1995)
51. Gill J C *J. Phys. C: Solid State Phys.* **19** 6589 (1986)
52. Ramakrishna S et al. *Phys. Rev. Lett.* **68** 2066 (1992)
53. Maher M P et al. *Phys. Rev. Lett.* **68** 3084 (1992); *Phys. Rev. B* **52** 13850 (1995)
54. Zaitsev-Zotov S V *Solid State Commun.* **76** 17 (1990)
55. Zaitsev-Zotov S V *Pis'ma Zh. Eksp. Teor. Fiz.* **46** 453 (1987) [*JETP Lett.* **46** 572 (1987)]
56. Zaitsev-Zotov S V *Synthetic Met.* **29** F433 (1989)
57. Gill J C *Phys. Rev. Lett.* **70** 331 (1993)
58. Higgs A W, in *Charge Density Waves in Solids: Proc. of the Intern. Conf., Budapest, Hungary, Sept. 3–7, 1984* (Lecture Notes in Physics, Vol. 217, Eds G Hutiray, J Sylyom) (Berlin: Springer-Verlag, 1985) p. 422
59. Mihály G, Mihály L *Phys. Rev. Lett.* **52** 149 (1984)
60. Zaitsev-Zotov S V *Synthetic Met.* **43** 3923 (1991)
61. Zaitsev-Zotov S V *Synthetic Met.* **56** 2623 (1993)
62. Cava R J et al. *Phys. Rev. Lett.* **53** 1677 (1984)
63. Yetman P J, Gill J C *Solid State Commun.* **62** 201 (1987)
64. Zaitsev-Zotov S V, Pokrovskii V Ya *Pis'ma Zh. Eksp. Teor. Fiz.* **49** 449 (1989) [*JETP Lett.* **49** 514 (1989)]
65. Pokrovskii V Ya, Zaitsev-Zotov S V *Europhys. Lett.* **13** 361 (1990)
66. Zaitsev-Zotov S V, Pokrovskii V Ya, Gill J C *J. Phys. I* (France) **2** 111 (1992)
67. Adelman T L, Zaitsev-Zotov S V, Thorne R E *Phys. Rev. Lett.* **74** 5264 (1995)
68. Pokrovskii V Ya, Zaitsev-Zotov S V, Monceau P *Phys. Rev. B* **55** R13377 (1997)
69. Pokrovskii V Ya, Zaitsev-Zotov S V *Phys. Rev. B* **61** 13261 (2000)
70. Pronin A V et al. *Physica B* **244** 103 (1998)
71. Mantel O C "Mesoscopic charge density wave wires", PhD Thesis (Delft: Technische Univ. Delft, 1999)
72. Zaitsev-Zotov S V, Slot E, van der Zant H S J *J. Phys. IV* (France) **12** Pr9-115 (2002)
73. Zaitsev-Zotov S V, to be published
74. Zaitsev-Zotov S V *Microelectron. Eng.* **69** 549 (2004)
75. Slot E, van der Zant H S J *J. Phys. IV* (France) **12** Pr9-103 (2002)
76. Zaĭtsev-Zotov S V, Pokrovskiĭ V Ya, Monceau P *Pis'ma Zh. Eksp. Teor. Fiz.* **73** 29 (2001) [*JETP Lett.* **73** 25 (2001)]
77. Zaitsev-Zotov S V et al. *Phys. Low-Dim. Struct.* (1/2) 79 (2002)
78. Mantel O C et al. *Phys. Rev. Lett.* **84** 538 (2000)
79. Latyshev Yu I et al. *Phys. Rev. Lett.* **78** 919 (1997)
80. Gill J C *Phys. Rev. Lett.* **65** 271 (1990)
81. Thorne R E, McCarten J *Phys. Rev. Lett.* **65** 272 (1990)
82. Itkis M E, Nad' F Ya *Pis'ma Zh. Eksp. Teor. Fiz.* **39** 373 (1984) [*JETP Lett.* **39** 448 (1984)]
83. Pouget J P et al. *Phys. Scripta* **T25** 58 (1989)
84. Moudden A H et al. *Phys. Rev. Lett.* **65** 223 (1990)
85. Richard J et al. *J. Phys.* (Paris) **44** C3-1685 (1977)
86. Thorne R E, private communication
87. Latyshev Yu I et al. *Physica B + C* **143** 155 (1986)
88. Zaĭtsev-Zotov S V, Pokrovskiĭ V Ya, in *Tezisy Dokladov XXV Vsesoyuznoĭ Konf. po Fizike Nizkikh Temperatur* (Abstracts of Papers Presented at the 25th All-Union Conf. in Low-Temperature Physics) Pt. 3 (Leningrad, 1988) p. 112
89. Pokrovskii V Ya, Zaitsev-Zotov S V *Synthetic Met.* **43** 3899 (1991)
90. Artemenko A N *J. Phys. IV* (France) **12** Pr9-77 (2002)
91. Monceau P, Richard J, Renard M *Phys. Rev. Lett.* **45** 43 (1980)
92. Fisher B *Solid State Commun.* **46** 227 (1983)
93. Latyshev Yu I, Savitskaya Ya S, Frolov V V *Pis'ma Zh. Eksp. Teor. Fiz.* **38** 446 (1983) [*JETP Lett.* **38** 541 (1983)]
94. Hutiráy Gy, Mihály G, Mihály L *Solid State Commun.* **43** 737 (1982)
95. van Kampen N G, in *Statistical Physics: Proc. of the IUPAP Intern. Conf.* (Eds L Pel, P Szepfanzy) (Amsterdam: North-Holland, 1976)
96. Artemenko S N, Volkov A F, in *Charge Density Waves in Solids* (Modern Problems in Condensed Matter Sciences, Vol. 25, Eds L P Gor'kov, G Grüner) (Amsterdam: North-Holland, 1989)
97. Artemenko S N *Zh. Eksp. Teor. Fiz.* **111** 1494 (1997) [*JETP* **84** 823 (1997)]
98. Artemenko S N et al. *Pis'ma Zh. Eksp. Teor. Fiz.* **39** 258 (1984) [*JETP Lett.* **39** 308 (1984)]
99. Forró L et al. *Phys. Rev. B* **34** 9047 (1986)
100. Ong N P, Brill J W *Phys. Rev. B* **18** 5265 (1978)
101. Brazovskii S, Matveenko S *Synthetic. Met.* **56** 2696 (1993)
102. Matsukawa H, Takayama H *J. Phys. Soc. Jpn.* **56** 1507 (1987)
103. Matsukawa H *J. Phys. Soc. Jpn.* **56** 1522 (1987)
104. Gill J C *J. Phys.: Condens. Matter* **1** 6649 (1989)
105. Mihály G, Canfield P *Phys. Rev. Lett.* **64** 459 (1990)
106. Bogachek E N et al. *Phys. Rev. B* **42** 7614 (1990)
107. Wind S et al. *Phys. Rev. Lett.* **57** 633 (1986)
108. Imry Y *Introduction to Mesoscopic Physics* (New York: Oxford Univ. Press, 1997) [Translated into Russian (Moscow: Fizmatlit, 2002)]
109. Artemenko S N *Phys. Rev. B* **67** 125420 (2003)
110. Voit J *Rep. Prog. Phys.* **58** 977 (1995)
111. Balents L, cond-mat/9906032
112. Gong Y et al. *Phys. Rev. B* **51** 12975 (1995)
113. Turgut S, Falicov L M *Phys. Rev. B* **49** 14043 (1994)
114. Nattermann Th, Giamarchi Th, Le Doussal P, cond-mat/0303233
115. Hillenius S J et al. *Phys. Rev. B* **23** 1567 (1981)
116. Zhilinskii S K et al. *Zh. Eksp. Teor. Fiz.* **85** 362 (1983) [*Sov. Phys. JETP* **58** 211 (1983)]